frontiers in Molecular Biosciences

TYPE Original Research
PUBLISHED 03 November 2026
DOI 10.3389/fmolb.2026.1922984

Check for updates

OPEN ACCESS

EDITED BY
Rahul Tyagi,
National Institutes of Health,
United States

REVIEWED BY
Cherine Charfeddine,
Pasteur Institute of Tunis, Tunisia
Eamon P McCarron,
The University of Sheffield,
United Kingdom

*CORRESPONDENCE
Maryada Sharma,
maryada24@yahoo.com

RECEIVED 29 June 2026
REVISED 16 September 2026
ACCEPTED 16 September 2026
PUBLISHED 03 November 2026

CITATION
Arora R, Panda NK, Virk RS, Bakshi J, Dogra M, Kaushik S and Sharma M (2026) Genotype-phenotype studies in neurosensory diseases: a blood based personalized disease modeling platform for neurosensory hearing loss. *Front. Mol. Biosci.* 13:1922984. doi: 10.3389/fmolb.2026.1922984

COPYRIGHT
© 2026 Arora, Panda, Virk, Bakshi, Dogra, Kaushik and Sharma. This is an open-access article distributed under the terms of the Creative Commons Attribution License (CC BY). The use, distribution or reproduction in other forums is permitted, provided the original author(s) and the copyright owner(s) are credited and that the original publication in this journal is cited, in accordance with accepted academic practice. No use, distribution or reproduction is permitted which does not comply with these terms.

# Genotype-phenotype studies in neurosensory diseases: a blood based personalized disease modeling platform for neurosensory hearing loss

Rhythm Arora[1], Naresh Kumar Panda[1], Ramandeep Singh Virk[1], Jaimanti Bakshi[1], Mohit Dogra[2], Shubham Kaushik[3] and Maryada Sharma[1]*

[1]Department of Otolaryngology and Head & Neck Surgery, Postgraduate Institute of Medical Education and Research, Chandigarh, India, [2]Department of Advanced Eye Centre, Postgraduate Institute of Medical Education and Research, Chandigarh, India, [3]Paris Lodron University of Salzburg, Salzburg, Austria

**Background:** Genetic testing has substantially improved the diagnosis of sensorineural hearing loss (SNHL); however, genomic findings alone often fail to explain patient-specific functional phenotypes, particularly in cases involving variants of uncertain significance (VUSs) or genetically unresolved disease. We evaluated whether an in-house Plasma-Induced Transcriptomic and epi-Transcriptomic Reprogramming (PITTRep) platform could bridge this gap by providing a functional, patient-specific model of disease biology.

**Methods:** Following validation of PITTRep as a reproducible plasma-driven transdifferentiation platform using autologous plasma and peripheral blood cells, seven clinically distinct SNHL cases were investigated, comprising hereditary POU3F4-associated hearing loss, MYO7A-associated congenital SNHL, three GJB2-associated cases representing truncating and missense variants with distinct clinical phenotypes, FGF3-associated congenital hearing loss, and acquired ototoxic SNHL without detectable pathogenic variants. Patient-derived blood cultures were evaluated using immunofluorescence, genomic and regulatory analyses, and phenotypic assessment of adipocyte-to-neurogenic transdifferentiation (ATN).

**Results:** Despite distinct clinical presentations and genetic backgrounds, all seven cases demonstrated a reproducible disruption of the ATN continuum. Healthy controls consistently underwent adipogenic niche formation followed by neuronal differentiation with organized neurite networks, whereas patient-derived cultures exhibited arrested adipogenic remodelling, compact cellular aggregates, reduced neuronal marker expression, and impaired neurite development. In the MYO7A case, functional remodelling occurred predominantly through untranslated regulatory regions, developmental transcription factors, long non-coding RNAs, and chromosome 11-associated sensory-developmental pathways while the coding variant remained unchanged. The ototoxic case revealed similar impairment of ATN despite the absence of pathogenic genomic variants, demonstrating persistent neuroinflammatory activation and defective neurogenic plasticity independent of inherited mutations. In contrast, POU3F4-associated cultures exhibited partial functional

rescue following artificial endolymph supplementation, highlighting the influence of microenvironmental modulation.

**Conclusion:** PITTRep reproducibly models patient-specific functional phenotypes across hereditary and acquired SNHL and identifies disruption of the adipocyte-to-neurogenic transdifferentiation continuum as a common systems-level feature of auditory dysfunction. These findings demonstrate the potential of PITTRep to complement genomic diagnostics by functionally interpreting disease-associated variants, stratifying genomically unresolved cases, and providing a scalable platform for precision diagnostics and regenerative medicine.

KEYWORDS

**adipocyte to neurogenic transition(ATN), neurogenic plasticity, neurosensory disease, patient-derived neurovascular model, PITTRep based disease modelling, regenerative medicine, sensorineural hearing loss, regulatory plasticity**

# Introduction

## Patient-specific organoids as next-generation functional diagnostics

The rapid advancement of genomic technologies has revolutionised the diagnosis of human diseases, enabling the identification of causative mutations across a wide spectrum of disorders, including sensorineural hearing loss (SNHL). However, despite the detection of pathogenic or likely pathogenic variants, a fundamental gap persists between genotype and functional phenotype. In many patients, especially those with heterogeneous or novel variants, genetic diagnosis fails to explain which cellular pathways are disrupted, how signalling networks are altered, or what therapeutic strategies may be effective. Moreover, even when a molecular diagnosis is established, the relationship between the identified variant and the observed clinical phenotype may remain incompletely understood, particularly in disorders with substantial genetic and phenotypic heterogeneity (Urizar et al., 2025). In hearing disorders, differences in clinical severity and disease trajectory across phenotypic and genotypic backgrounds further highlight the challenges of establishing robust genotype–phenotype correlations (McCarron et al., 2026).

This challenge is particularly evident in disorders of the inner ear, where direct access to human tissue is extremely limited. As a result, our understanding of disease mechanisms has historically relied on animal models or simplified *in vitro* systems, which often fail to recapitulate human-specific developmental and physiological processes (van der Valk et al., 2021; Pianigiani and Roccio, 2024). While these models have provided valuable insights, their translational relevance remains constrained, especially in the context of patient-specific variability.

In this context, organoid technology has emerged as a transformative platform bridging the gap between molecular diagnosis and functional biology. Organoids are three-dimensional, self-organising structures derived from stem cells that recapitulate key aspects of tissue architecture, cellular diversity, and physiological function. Recent advances in induced pluripotent stem cell (iPSC)-derived organoids have enabled the generation of human inner ear–like structures containing hair cells, supporting cells, and neuronal components, closely mimicking *in vivo* development and function (Roccio and Edge, 2019; Pianigiani and Roccio, 2024). These systems provide, for the first time, an opportunity to study disease-relevant cell types derived directly from patients.

Importantly, patient-specific organoids extend beyond disease modelling to enable functional diagnostics. By integrating patient-derived cells with controlled microenvironmental cues, these systems allow interrogation of mutation-specific effects on developmental trajectories, signalling pathways (e.g., Wnt, Notch), electrophysiological properties, and cellular fate decisions. Furthermore, they offer a platform for drug screening, gene correction validation, and personalised therapeutic testing, thereby addressing the critical question: what next after identifying a genetic variant (Roccio and Edge, 2019; Pianigiani and Roccio, 2024; Lou et al., 2025)?

Despite these advances, current organoid models still face significant limitations. Many systems lack full cellular complexity, vascularisation, and long-term maturation, and may not fully replicate *in vivo* microenvironments or systemic interactions (Fan et al., 2025). In inner ear organoids, challenges include incomplete cochlear maturation, variability in differentiation efficiency, and limited representation of diverse supporting cell types and neuro-glial interactions. Additionally, most existing studies focus on generalised disease modelling rather than on true patient-specific diagnostic applications, leaving a critical gap in translational implementation (van der Valk et al., 2021; Fan et al., 2025).

Therefore, there is an urgent need to develop next-generation patient-specific organoid platforms that integrate genetic, molecular, and functional data to enable:

1. Decoding the functional consequences of genetic variants,
2. Identifying disrupted signalling pathways and cellular phenotypes,
3. Stratifying patients beyond genotype into functional subtypes, and
4. Guiding personalised therapeutic interventions, even in genetically unresolved cases.

In this study, we propose that patient-specific organoid systems, particularly those derived from accessible sources such as blood,

can serve as a clinically relevant, scalable, and minimally invasive diagnostic platform, bridging the gap between genomics and precision medicine. Such models have the potential to redefine diagnostics by shifting from mutation identification to functional interpretation, ultimately enabling actionable insights for complex and heterogeneous disorders like SNHL.

# Methodology

## Ethics statement

The study involving patients and controls was approved by the Institutional Ethics Intramural Committee of the Postgraduate Institute of Medical Education and Research, IEC no: IEC-INT/2024/PhD-1585. Postgraduate institute of medical education and research, (PGIMER), Chandigarh, India. The studies were conducted in accordance with the local legislation and institutional requirements. Written informed consent for participation in this study was provided by the participant's legal guardians/next of kin.

## Study design and patient cohort

This study was designed to explore the feasibility of integrating patient-specific PITTRep-derived phenotypic characterization with clinical and genomic information in sensorineural hearing loss (SNHL). Seven patients with clinically heterogeneous SNHL were evaluated using patient-derived PITTRep cultures, clinical phenotyping, and case-specific genomic investigations. The cohort included hereditary and genetically unresolved forms of hearing loss involving POU class 3 homeobox 4 (POU3F4), myosin VIIA (MYO7A), gap junction beta-2 (GJB2), and fibroblast growth factor 3 (FGF3) as well as an acquired ototoxicity-associated hearing-loss phenotype without an identified disease-associated variant.

Case 1 was a 7-year-old male with congenital severe and progressive SNHL and a family history consistent with X-linked inheritance. Genetic evaluation identified a pathogenic POU3F4 variant. Additional affected and unaffected family members were investigated for familial segregation and comparative analysis. The proband underwent cochlear implantation.

Case 2 was a 3-year-old female with congenital profound bilateral hearing loss. Comprehensive genomic investigations identified a homozygous MYO7A variant classified as a variant of uncertain significance (VUS). Sanger sequencing and clinical whole-genome sequencing were subsequently performed to further characterize the genomic findings. Both parents were included as familial controls.

Case 3 was a 4-year-old male with post-lingual bilateral SNHL, with hearing impairment developing at approximately 3 years of age following clinically documented drug-associated ototoxic exposure. WES did not identify a significant phenotype-associated variant. The patient therefore provided a genetically unresolved, acquired form of hearing loss for functional comparison within the PITTRep system. Both parents were included as familial controls.

Cases 4–6 represented additional patients with GJB2-associated hearing loss. Case 4 was a 5-year-old male carrying a truncating GJB2 variant, whereas Cases 5 and 6 were a 3-year-old male, carrying the same missense GJB2 variant. Cases 5 and 6 were maternally related cousins, with Case 6, a 3-year-old female, being the maternal cousin of Case 5.

Case 7 was a 1-year-old male with an FGF3-associated genetic finding. WES identified an FGF3 variant, providing an additional genetic context distinct from the POU3F4, MYO7A, and GJB2-associated cases.

The seven cases were therefore selected to encompass distinct genetic and clinical contexts while allowing assessment of whether alterations in the adipocyte-to-neurogenic transdifferentiation (ATN) continuum could be observed across genetically diverse forms of SNHL and an acquired ototoxic phenotype. The expanded cohort was intended to strengthen the proof-of-concept assessment of PITTRep as a patient-specific functional disease-modelling platform rather than to establish definitive genotype–phenotype correlations or clinical diagnostic performance.

Control selection was primarily family-based. For Case 1, affected male siblings and unaffected parents were available for comparative and segregation analyses. For Case 2, both parents were included as healthy familial controls. For Case 3, both parents were similarly used as familial controls. For the additional GJB2- and FGF3-associated cases, available familial relationships and samples were incorporated where applicable. Age-matched unaffected siblings were not available fo and recruitment of additional healthy age-matched pediatric participants was not permitted under the approved study protocol because of the young age of the participants. Accordingly, parental or available familial samples were used as controls where appropriate. The detailed clinical and genetic characteristics of all seven cases are summarized in Table 1.

## PITTRep culture system

The PITTRep culture system (Patent Application No. 202411034351), previously described in detail by Sharma et al. (2022a) and Arora et al. (2025), was employed for patient-specific functional modelling. Peripheral blood samples were collected from patients and healthy control donors following ethical approval and informed consent.

Autologous blood components were separated using a density gradient-based layering method. Briefly, diluted whole blood (1:1 with RPMI 1640) was layered over HiMedia Hisep 1077 and Granulosep 1119 (1:1:3 ratio) and centrifuged at 2000 rpm for 40 min. Peripheral blood mononuclear cells (PBMCs) and granulocyte fractions were collected, washed with phosphate-buffered saline (PBS), and resuspended.

All cells, including RBCs (4 µL/mL), were added and cultured in autologous plasma in 24-well plates. Cultures were maintained for 14 days at 37 °C in a humidified 5% $CO_2$ incubator and monitored using brightfield microscopy.

PITTRep cultures were evaluated in two spatially distinct microenvironments: the coverslip-associated region representing a normoxic environment and the well region beneath the coverslip representing a hypoxic environment (Supplementary Figure S10).

TABLE 1 Detailed clinical, phenotypic, and genomic characteristics of the seven cases.

| Parameter | Case 1 | Case 2 | Case 3 | Case 4 | Case 5 | Case 6 | Case 7 |
|---|---|---|---|---|---|---|---|
| Sex | Male | Female | Male | Male | Male | Female | Male |
| Age at recruitment | 7 years | 3 years | 4 years | 5 years | 3 years | 3 years | 1 year |
| Hearing-loss onset | Congenital | Congenital | ~3 years | Congenital | Congenital | Congenital | Congenital |
| Clinical phenotype | Severe progressive SNHL | Profound congenital hearing loss | Post-lingual hearing loss | Profound congenital hearing loss | Profound congenital hearing loss | Profound congenital hearing loss | Profound congenital hearing loss (Michel's aplasia) |
| Primary genetic test | WES | WES | WES | WES | WES | WES | WES |
| WES platform | Illumina | MGI | Illumina | Illumina NovaSeq | Illumina NovaSeq | Illumina NovaSeq | Illumina NovaSeq |
| WES reference genome | GRCh37/hg19 | GRCh37/hg19 | GRCh37/hg19 | GRCh37/hg19 | GRCh37/hg19 | GRCh37/hg19 | GRCh38/hg38 |
| Gene | POU3F4 | MYO7A | No variant identified | GJB2 | GJB2 | - | FGF3 |
| Variant | c.862_865del; p.Val289ArgfsTer47 | c.5498G>A; p.Gly1833Asp | — | c.71G>A; p.Trp24Ter | c.551G>A; p.Arg184Gln | - | c.534C>G; p.Phe178Leu |
| Variant type | Frameshift | Missense | — | Nonsense/ truncating | Missense | - | Missense |
| Zygosity | Hemizygous | Homozygous | — | Not specified | Not specified | - | Not specified |
| Classification | Pathogenic | VUS | — | Not specified | Not specified | - | Not specified |
| Additional samples analysed | 2 affected male siblings; mother (carrier); father (unaffected) | Mother and father as healthy controls | Mother and father as healthy controls | Not specified | Maternal family relationship with Case 6 | Maternal cousin of Case 5 | Not specified |
| Additional genomic testing | Targeted MPS | Sanger + WGS | — | Not specified | Not specified | Not specified | Not specified |
| Familial/variant validation | Targeted MPS/segregation | Sanger | — | Not specified | Not specified | Not specified | Not specified |
| WGS platform | — | Illumina | — | — | — | — | — |
| WGS reference genome | — | GRCh38/hg38 | — | — | — | — | — |

## Artificial endolymph supplementation and auditory stimulation

This experiment was performed specifically for Case 1, given the established association of POU3F4 with inner-ear structures involved in cochlear development and auditory homeostasis, including the stria vascularis and outer hair cell-associated compartments. Because the stria vascularis plays a central role in maintaining the ionic composition and electrochemical properties of the endolymph, an artificial endolymph exposure was introduced as an exploratory experimental condition to examine whether modulation of the extracellular ionic environment was associated with differences in the patient- and family-derived PITTRep phenotypes.

To investigate the response of the PITTRep-derived cultures to an endolymph-like ionic environment, an artificial endolymph solution was prepared containing 140 mmol/L KCl and 25 mmol/L $KHCO_3$. For preparation of 50 mL solution, 521.85 mg KCl and 125.14 mg $KHCO_3$ were used.

On day 8 of culture, the existing plasma-containing culture medium was removed from the designated wells and replaced with 1 mL of the artificial endolymph solution. Parallel cultures

maintained under the standard PITTRep condition without endolymph replacement served as the untreated control condition. This experimental comparison was performed for the proband, both affected siblings, and their parents, allowing assessment of the response across the different members of the family.

Following replacement with the artificial endolymph solution, the cultures were exposed to OM sound as an auditory/music stimulus. The endolymph exposure was maintained for 6 h, after which the culture solution was removed, and the cells were immediately fixed with 4% paraformaldehyde for subsequent immunofluorescence analysis. Control and endolymph-treated cultures were processed in parallel using the same fixation and immunofluorescence protocol.

## Replicate structure

For each case, PITTRep cultures were established from one patient-derived sample and, where available, one mother-derived and one father-derived sample. In Case 1, an additional affected brother-derived sample was included. Each donor was represented by a single culture, and no independent replicate cultures or technical replicate wells were performed. For each experimental condition and immunofluorescence assay, a single culture was analysed per donor. As the study participants were young children, collection of additional blood samples was not considered clinically appropriate or feasible, limiting the availability of additional biological material for independent replicate cultures. Thus, the number of biological samples corresponds to the number of individual donors included in each case, with no technical replicates.

## Immunofluorescence

Cells and tissue were fixed with 4% paraformaldehyde (PFA) for 10 min, followed by treatment by 0.3% Triton X-100 for 5–10 min and blocked using a freshly prepared blocking solution (2.5% BSA) for 2 h.

Cells were then incubated with primary antibodies for 16 h at the following dilutions: c-Kit (rabbit, Cell Signaling Technology, 3074S, 1:500), Stargazin (mouse, Invitrogen), ionized calcium-binding adapter molecule 1 (IBA-1) (rabbit, Invitrogen, MA5-29012, 1:500), glial fibrillary acidic protein (GFAP) (mouse, Invitrogen, MA515086, 1:500), vesicular glutamate transporter 2 (VGLUT2) (mouse, Invitrogen, MA527613, 1:500), myosin VIIA (MYO7A) (mouse, Santa Cruz Biotechnology, sc-74516, 1:500), gastrulation brain homeobox 2 (GBX2) (goat, Invitrogen, PA5-18561, 1:600), alpha-smooth muscle actin (α-SMA) (rabbit, Invitrogen, PA5-87638, 1:500), sarco/endoplasmic reticulum $Ca^{2+}$-ATPase 2 (SERCA2) (mouse, Abcam, AB2817, 1:500), msh homeobox 2 (MSX2) (rabbit, Invitrogen, PA5-106670, 1:500), mature BDNF polyclonal antibody (rabbit, Osenses, OSB00032W-100UL), and tropomyosin receptor kinase B (TrkB) antibody (goat, Bio-Techne, AF1494).

The cells were washed with PBS twice, with each wash lasting 2 min. After this, secondary antibodies were added against the primary antibodies for 2 h. The antibodies used were goat Alexa Fluor 488 and 568 and donkey Alexa Fluor 647 conjugates (Invitrogen, 1:200) and Alexa Fluor 647 Phalloidin (Invitrogen, 1:500).

After the completion of secondary antibody incubation, the cells were washed again with PBS two times. Then DAPI (1:20) was added and incubated for 15 min. A thorough wash was performed after the completion of incubation.

At last, the cells were mounted with 70% glycerol.

## Statistical analysis

Immunofluorescence images were quantitatively assessed by measuring mean fluorescence intensity (MFI) using Fiji/ImageJ. For each image, background fluorescence was subtracted from the measured MFI to obtain background-corrected fluorescence values. For the paired culture-condition experiment in Case 1 (POU3F4-associated hearing loss), background-corrected fluorescence values obtained from each donor under standard PITTRep culture were used as the within-donor reference (normalized to 1.0), and the corresponding values following artificial endolymph supplementation were expressed relative to the matched standard-culture value. As each donor was represented by a single culture without independent technical replicate wells, immunofluorescence measurements from the individual cases were primarily interpreted descriptively. For Case 1, the normalized fluorescence values from the same four donors (patient, affected brother, mother, and father) under standard and artificial endolymph conditions were compared using a two-tailed paired Student's t-test, with each donor serving as a matched pair. A $p$ value $< 0.05$ was considered statistically significant. Given the limited number of biological samples, this statistical comparison was considered exploratory. Quantitative immunofluorescence measurements and corresponding normalization analyses are provided in the Supplementary Material.

## Whole-exome sequencing (WES)

Whole-exome sequencing (WES) was performed for all seven patients as part of their clinical genetic evaluation through accredited external diagnostic laboratories. Genomic DNA was isolated from peripheral blood collected in EDTA tubes and subjected to targeted enrichment of protein-coding regions and clinically relevant splice-junction regions using validated capture-based NGS workflows. Because sequencing and primary bioinformatic analyses were performed through external diagnostic facilities at different time points, laboratory-specific capture systems, sequencing platforms, and validated analytical pipelines were used.

For Case 1 (POU3F4-associated hearing loss) and Case 3 (ototoxicity-associated hearing loss), WES was performed using Illumina sequencing with paired-end reads (2 × 100 or 2 × 150 bp) following targeted exome enrichment. Sequence reads were aligned to the GRCh37/hg19 human reference genome and analysed using phenotype-driven laboratory-validated bioinformatic pipelines. For Case 2 (MYO7A-associated hearing loss), WES was performed using a targeted gene-capture system with sequencing on an MGI platform, with a mean sequencing depth exceeding 100×. Sequence data were aligned to GRCh37/hg19 and analysed using the laboratory's validated bioinformatic workflow. For Cases 4–6

(GJB2-associated hearing loss), WES was performed as part of clinical genetic evaluation using validated targeted exome-capture workflows on the Illumina NovaSeq platform. The corresponding datasets were analysed against the GRCh37/hg19 reference genome. Sequencing and primary bioinformatic analyses were performed by the respective external diagnostic laboratories using their validated laboratory-specific workflows. For Case 7, WES was performed using the Illumina NovaSeq platform, and the sequence data were analysed against the GRCh38/hg38 reference genome using the laboratory's validated bioinformatic pipeline.

Across all seven WES datasets, variant calling and annotation were performed using laboratory-validated bioinformatic pipelines incorporating established clinical and population databases, including ClinVar, Online Mendelian Inheritance in Man (OMIM), Single Nucleotide Polymorphism Database (dbSNP), Genome Aggregation Database (gnomAD), and Human Gene Mutation Database (HGMD), where available. Computational prediction tools were additionally applied according to the analytical workflow of the respective diagnostic laboratory for assessment of the potential functional consequences of identified variants.

Variants were prioritized on the basis of the patient's clinical phenotype, gene–disease association, inheritance pattern, population frequency, predicted molecular consequence, evolutionary conservation, available clinical evidence, and database annotations. Clinically relevant variants were interpreted according to established clinical variant-classification frameworks, including the American College of Medical Genetics and Genomics/Association for Molecular Pathology (ACMG/AMP) criteria where applicable. Variant classifications reported by the respective diagnostic laboratories were subsequently considered in conjunction with the patient's clinical phenotype, family history, and functional findings obtained using the PITTRep platform.

## Whole-genome sequencing (WGS)

Whole-genome sequencing (WGS) was performed for Case 2 (MYO7A-associated SNHL) through outsourced labs as an extended genomic investigation following whole-exome sequencing and variant confirmation. Genomic DNA extracted from the patient's blood sample was subjected to whole-genome sequencing on an Illumina platform, with a mean sequencing depth of approximately 30×. The sequencing generated approximately 88.13 Gb of data, with 99.98% of reads aligned and 97.11% of bases meeting the Q30 quality threshold.

Sequence reads were pre-processed and aligned to the human reference genome GRCh38 using the BWA aligner. Variant calling followed the GATK Best Practices framework implemented through Illumina DRAGEN, including read processing, duplicate removal, recalibration, and INDEL realignment. Single-nucleotide variants (SNVs) and small insertions/deletions (INDELs) were identified and subsequently annotated using the VariMAT pipeline. Gene and transcript-level annotation was performed using the Variant Effect Predictor (VEP) against the Ensembl release 99 human gene model.

In addition to SNVs and INDELs, copy-number variants (CNVs) were assessed using the CANVAS algorithm, which identifies genomic regions showing deviations in read depth relative to the expected coverage profile. Clinically relevant variants identified across coding and non-coding regions were annotated using disease-associated databases including ClinVar, OMIM, HGMD, LOVD, DECIPHER, and SwissVar. Population-frequency filtering incorporated 1000 Genomes Phase 3, gnomAD v3.1 and v2.1.1, dbSNP, TOPMed Freeze 8, GenomeAsia, and the MedVarDb v2.1 Indian population database.

Potential effects of non-synonymous variants were assessed using multiple *in silico* prediction tools, including PolyPhen-2, SIFT, MutationTaster2, and LRT. Clinically relevant variants were subsequently interpreted in the context of the patient's phenotype and classified according to the American College of Medical Genetics and Genomics (ACMG) framework used by the reporting laboratory.

The WGS analysis provided broader genomic interrogation than WES by enabling assessment of coding and non-coding genomic regions, including variants outside the regions primarily captured by exome sequencing. In the present case, WGS identified the previously observed homozygous MYO7A c.5498G>A (p.Gly1833Asp) variant, classified as a VUS. No additional pathogenic or likely pathogenic variant was identified that provided a definitive molecular explanation for the patient's phenotype.

## Massively parallel sequencing (targeted/clinical validation)

Massively parallel sequencing (MPS) was performed in Case 1 to confirm the POU3F4 variant identified by WES and to assess familial segregation. Peripheral blood samples collected in EDTA tubes were used for genomic DNA extraction. A targeted NGS assay was performed for POU3F4 (NM_000307.5), encompassing the candidate variant identified through WES. Sequencing and primary analysis were performed through an external accredited diagnostic laboratory using its validated targeted NGS workflow.

Sequence data were subjected to quality assessment, alignment to the relevant reference sequence, and targeted variant detection. Variant zygosity was assessed in the proband and available family members to evaluate allele transmission and segregation with the X-linked inheritance pattern. The targeted assay was used specifically to provide independent confirmation of the WES finding and to assess its segregation within the family.

## Sanger sequencing validation

Sanger sequencing was performed to independently validate the MYO7A variant identified by next-generation sequencing in Case 2. Genomic DNA extracted from peripheral blood was used as the template for PCR amplification of the genomic region encompassing the candidate MYO7A variant. The amplified target was subjected to capillary-based Sanger sequencing through an accredited external diagnostic laboratory. The resulting chromatograms were analysed against the corresponding reference sequence to verify the nucleotide change and determine its allelic state. Sanger sequencing was used as an orthogonal confirmation of the NGS-identified variant, providing an independent sequence-based assessment of the candidate MYO7A alteration.

## Multispectral optoacoustic tomography (MSOT) imaging

MSOT imaging was performed using the inVision 256-TF system (iThera Medical, Germany). The instrument employs a tunable optical parametric oscillator (OPO) pumped by an Nd:YAG laser, delivering excitation pulses of 9 ns duration over a wavelength range of 660–1300 nm at a repetition rate of 25 Hz and wavelength switching time of 10 m. Image reconstruction was carried out using viewMSOT version 5.3 software with the BP 5.0 preset. The reconstruction field of view was set to 25 mm, corresponding to an approximate spatial resolution of 75 µm.

### Phantom preparation

For MSOT imaging, PITTRep cultures were embedded in a low-temperature-gelling agarose phantom. Briefly, 0.75 g agarose was dissolved in 50 mL distilled water, PBS, or saline by heating until completely dissolved. Approximately 5 mL of the agarose solution was allowed to gel at the base of a modified 20-mL syringe, after which the washed culture was positioned on the gel and oriented to remove air bubbles. Additional agarose maintained at 37 °C was added to completely embed the culture, and the phantom was subsequently cooled to allow complete gelation before imaging.

### MSOT imaging/acquisition

Phantoms were positioned in the dedicated imaging holder and maintained in a water bath at 37 °C. Twenty frames per wavelength were acquired and averaged to improve image quality and reduce noise. Optoacoustic signals were collected at wavelengths of 660, 680, 700, 730, 760, 800, 850, and 875 nm. Hemoglobin-specific absorption peaks occur near 760 nm for deoxyhemoglobin (Hb) and 875 nm for oxyhemoglobin ($HbO_2$), while 800 nm represents the isosbestic point reflecting total hemoglobin.

## Bioinformatic analysis of regulatory variants and functional networks

To investigate regulatory alterations beyond coding variants, datasets from paired samples, including native whole blood (control) and patient-specific PITTRep-derived cultures (test), were subjected to whole-genome sequencing on an Illumina platform at a mean depth of approximately 30x. Variant calling was performed following the GATK best-practices framework as implemented in Illumina DRAGEN® (Zhao et al., 2020; Betschart et al., 2024). Raw sequencing reads were pre-processed and aligned to the human reference genome (GRCh38/hg38) using the BWA aligner (Li and Durbin, 2010; Zhao et al., 2020). Aligned reads were subsequently processed within DRAGEN for duplicate removal, base quality score recalibration (BQSR), and indel realignment (Zhao et al., 2020). Single-nucleotide variants (SNVs) and small indels were annotated using the VariMAT pipeline while gene-level annotations were performed using VEP program against the Ensembl release 99 human gene model (McLaren et al., 2010). Clinically relevant variants in both coding and non-coding regions are annotated using variants published in literature and a set of diseases databases: ClinVar, OMIM, HGMD, LOVD, DECIPHER (population CNV) and SwissVar (Amberger et al., 2009; Firth et al., 2009; Mottaz et al., 2010; Fokkema et al., 2011; Landrum et al., 2016; Stenson et al., 2017). Common variants were filtered against population allele frequencies reported in 1000 Genome Phase 3, gnomAD (v3.1 and v2.1.1), dbSNP (GCF_000001405.38), 1000 Japanese Genome, TOPMed (Freeze_8), Genome Asia, and the in-house Indian population database (MedVarDb v2.1) (1000 Genomes Project Consortium et al., 2015; GenomeAsia100K Consortium, 2019; Nagasaki et al., 2015; Sherry et al., 2001; Taliun et al., 2021; Wang et al., 2019). The effect of non-synonymous variants effect is predicted using multiple algorithms such as PolyPhen-2, SIFT, MutationTaster2 and LRT.

In parallel, whole-exome sequencing (WES) was performed on the same paired samples for confirmation of coding-region variants. Whole-exome libraries were prepared using the Agilent SureSelect XT HS2 target enrichment system with Human All Exon V8 probes, and captured fragments were purified using Dynabeads MyOne Streptavidin T1 magnetic beads. Library quality was assessed using an Agilent 4200/4150 TapeStation (HS D1000 ScreenTape assay), with concentration determined by Qubit fluorometry. Raw BCL files were converted to FASTQ format using DRAGEN® and subjected to quality assessment using FastQC (Andrews, 2010), followed by adapter trimming and quality filtering with Trimmomatic (Sherry et al., 2001; Bolger et al., 2014; Auton et al., 2015; Nagasaki et al., 2015). Filtered reads were aligned to the human reference genome (GRCh37/hg19) using BWA-MEM, and duplicate reads were marked using Picard tools ("Picard toolkit," 2019). Base Quality Score Recalibration (BQSR) was performed using GATK, referencing dbSNP, Mills, and 1000 Genomes indel resources, followed by variant calling using GATK HaplotypeCaller (Poplin et al., 2017) Raw VCF files were filtered using hard-filtering criteria or Variant Quality Score Recalibration (VQSR) to retain high-confidence calls and annotated using the VEP program against the Ensembl human gene model, consistent with the annotation strategy applied to the whole-genome dataset.

From the WGS dataset, variants were filtered to focus on regulatory regions, particularly untranslated regions (5′UTR and 3′UTR) and intronic elements associated with gene regulation. A comparative analysis between control and test samples was performed and variant enrichment was assessed statistically to identify unique and enriched variants in the cultured condition, enabling distinction between baseline polymorphisms and culture-induced regulatory signatures. Variants specifically enriched in the test condition were treated as candidate culture-associated regulatory signatures. Identified variants were classified according to the American College of Medical Genetics and Genomics (ACMG) guidelines (Richards et al., 2015a).

To understand the functional implications of these regulatory changes, enrichment analysis was carried out using publicly available gene set libraries through Enrichr (https://maayanlab.cloud/Enrichr/) (Kuleshov et al., 2016), with pathway annotations derived from WikiPathways (Marino et al., 2023; Agrawal et al., 2024). Pathways were prioritized based on statistical significance (adjusted p-value < 0.05), allowing identification of key biological processes associated with the observed regulatory variation.

In parallel, non-coding regulatory associations were explored using integrated databases, including LncHub2 (https://maayanlab.cloud/lncHUB2/) (Marino et al., 2023). Enrichr-linked

datasets, and NCBI resources, to assess the contribution of long non-coding RNA–mediated regulatory mechanisms.

To further characterise the global regulatory landscape, dimensionality reduction analysis was performed using Uniform Manifold Approximation and Projection (UMAP) UMAP through Appyters computational framework (Clarke et al., 2021). This enabled visualisation of structured clustering patterns corresponding to distinct regulatory and functional domains. Features and clusters were ranked based on statistical significance, facilitating identification of coordinated regulatory networks associated with the test condition.

# Results and discussion

## Establishment and validation of the plasma-driven PITTRep platform

To establish a patient-specific functional platform capable of translating peripheral molecular signatures into disease-relevant cellular phenotypes, we first validated the reproducibility of our plasma-driven transdifferentiation strategy across both immortalised monocytic cells and primary human blood cells. This work builds upon our previously developed Plasma-Induced Transcriptomic and Epitranscriptomic Reprogramming (PITTRep) platform (Patent No. 202411034351), which utilizes neat autologous plasma as the sole culture microenvironment without exogenous growth factors or genetic manipulation (Sharma et al., 2022a; Arora et al., 2025).

As an initial proof-of-concept, THP-1 monocytic cells cultured in neat plasma for 72 h underwent extensive transcriptomic remodelling, demonstrating significant enrichment of neuronal-associated biological processes, including olfactory transduction, taste transduction, GnRH signalling, and multiple pathways associated with neuronal differentiation and plasticity. These findings established that plasma-derived cues alone are sufficient to initiate lineage reprogramming toward a neuronal state (Sharma et al., 2022a) Similar observations supporting the plasticity of blood-derived cells and their ability to acquire neural characteristics under inductive microenvironments have also been reported previously (Brazelton et al., 2000; Mezey et al., 2000; Bellon et al., 2018).

To determine whether this phenomenon was reproducible in physiologically relevant primary cells, peripheral blood mononuclear cells (PBMCs) isolated from healthy donors were cultured in autologous plasma and compared with conventional RPMI supplemented with 10% fetal bovine serum. Similar to the monocytic model, plasma-cultured PBMCs consistently exhibited enrichment of neuronal developmental pathways and neurogenic transcriptional programs, confirming that plasma-mediated transdifferentiation extends beyond immortalized cell lines to primary human cells (Arora et al., 2025).

The transcriptomic findings were further supported by phenotypic characterisation. Immunocytochemical analyses demonstrated robust expression of canonical neuronal markers, including NeuN, βIII-tubulin, VGLUT2, Stargazin, and DBH, while complementary cytochemical staining revealed neurite-like extensions, neuronal morphology, and myelin-like structural features, collectively supporting progressive neuronal maturation (Arora et al., 2025) The coordinated expression of these markers is consistent with established indicators of neuronal differentiation and synaptic maturation reported in previous studies (Horschitz et al., 2010; Meka et al., 2019; Hobert, 2021; Hilton et al., 2024; Bohlson and Tenner, 2025).

These findings demonstrated that plasma exposure was associated with transcriptomic changes enriched for neuronal-associated processes, using autologous human blood. By generating patient-specific neuronal phenotypes directly from peripheral blood, PITTRep provides a functional bridge between circulating molecular alterations and disease-associated cellular behavior. This framework therefore offers a unique opportunity to investigate individual disease mechanisms in clinically heterogeneous disorders (Sharma et al., 2022a; Arora et al., 2025).

Building on this validated platform, we next applied PITTRep to blood samples obtained from patients with sensorineural hearing loss to determine whether disease-specific molecular programs are retained during plasma-mediated transdifferentiation and can be functionally modelled *in vitro*.

## Patient-specific PITTRep cultures reveal altered adipocyte-to-neurogenic remodelling

Having established the robustness of the PITTRep platform in healthy blood-derived systems, we next investigated whether plasma-mediated transdifferentiation could capture disease-associated functional alterations in patients with sensorineural hearing loss (SNHL). To address this, we evaluated seven clinically distinct patient cases representing different etiologies of hearing impairment and compared their cellular remodelling trajectories with those of healthy controls cultured under identical conditions.

Despite their diverse clinical presentations, all patient-derived cultures exhibited a strikingly conserved biological phenotype characterised by disruption of the adipocyte-to-neurogenic transdifferentiation (ATN) continuum. Whereas healthy control cultures reproducibly underwent sequential adipogenic expansion, cellular remodelling, and the subsequent emergence of mature neuron-like networks, patient-derived cultures consistently demonstrated impaired progression through this developmental trajectory. Instead, cultures were characterised by the formation of small, fragmented, or prematurely arrested cellular clusters, with reduced structural organisation and limited neuronal maturation. These observations are consistent with growing evidence that successful lineage plasticity depends upon coordinated regulation of cellular remodelling, developmental signalling, cytoskeletal organization, and neurogenic commitment (Zuk et al., 2002; Jumabay et al., 2012; Gascón et al., 2017; Vasan et al., 2021).

These observations suggest that defective adipogenic remodelling represents a shared functional abnormality across genetically and clinically heterogeneous forms of hearing loss. Rather than reflecting disease-specific morphological differences alone, the PITTRep platform identified a convergent impairment in cellular plasticity that ultimately compromised neurogenic differentiation.

The following case reports illustrate how this common functional phenotype manifested across seven independent

patient samples, highlighting both their individual clinical characteristics and the shared disruption of adipocyte-to-neurogenic transdifferentiation.

## Patient-specific neurodevelopmental modeling of POU3F4-associated hearing loss

### Case study I: bilateral congenital severe profound sensorineural hearing loss associated with a POU3F4 variant

A 7-year-old male presented with prelingual bilateral severe-to-profound sensorineural hearing loss (SNHL), confirmed by brainstem evoked response audiometry (BERA), with absence of auditory responsiveness since infancy and progressive deterioration of hearing function. Family history revealed multiple affected males within the maternal lineage, strongly suggesting an inherited X-linked auditory disorder. Pedigree analysis demonstrated a classical X-linked inheritance pattern with unaffected paternal transmission and maternal carrier status (Figure 1A). Whole-exome sequencing subsequently identified a hemizygous pathogenic variant in POU3F4, which was validated in both affected siblings through massive parallel sequencing (Figures 1B,C), thereby establishing a definitive molecular diagnosis.

POU3F4 encodes a developmental transcription factor essential for mesenchymal patterning of the cochlea, spiral ligament fibrocyte maturation, neural crest-associated differentiation, and formation of stria vascularis-associated structures required for maintenance of potassium-rich endolymph and the endocochlear potential (De Kok et al., 1995; Phippard et al., 1999; Braunstein et al., 2008). Unlike primarily mechanotransduction-associated mutations restricted to cochlear hair cells, POU3F4-associated pathology involves disruption of broader developmental and ionic homeostatic systems governing peripheral auditory microenvironment stability. Consequently, although genomic sequencing establishes the genetic basis of disease, it does not by itself reveal how the variant is reflected at the cellular level or whether patient-derived cells retain measurable phenotypic responses to environmental modulation (Sharma et al., 2022a; Arora et al., 2025). These observations are particularly relevant to POU3F4-associated hearing loss because melanocyte-like intermediate cells within the stria vascularis arise from neural crest-derived developmental programs and contribute to the maintenance of cochlear ionic homeostasis (Groves and Fekete, 2012; Basch et al., 2016a).

Based on these observations and the established role of POU3F4 in inner-ear development and cochlear homeostasis, we hypothesized that the patient-associated cellular phenotype might be modifiable by changes in the extracellular ionic environment (De Kok et al., 1995; Phippard et al., 1999; Braunstein et al., 2008).

To test this hypothesis, we established patient-specific PITTRep cultures using autologous blood-derived samples from the proband, affected sibling, and both parents. The inclusion of the two affected siblings, a heterozygous carrier mother, and a non-carrier father provided a within-family comparison for examining cellular phenotypes in relation to the POU3F4 genotype. The PITTRep platform, previously shown to generate donor-specific neurovascular tissue-like structures under plasma-driven conditions, was therefore used to examine patient-associated cellular organization and marker expression under standard and altered ionic conditions (Sharma et al., 2022a; Arora et al., 2025).

Given the established role of POU3F4 in inner-ear development and its association with structures involved in cochlear ionic homeostasis, particularly the spiral ligament fibrocytes and stria vascularis, we examined whether altering the extracellular ionic environment could modify the patient-derived cellular phenotype. Artificial endolymph supplementation was therefore introduced into the PITTRep culture system on day 8 to provide a potassium-rich ionic environment relevant to cochlear endolymph. The artificial endolymph was maintained in the cultures for 6 h, after which the cultures were fixed for immunofluorescence analysis. This experimental perturbation was performed specifically for the POU3F4-associated case because of the established involvement of POU3F4 in cochlear developmental pathways and structures associated with endolymphatic homeostasis (Wangemann, 2006; Hibino et al., 2010; Basch et al., 2016b; Nin et al., 2016; Bovee et al., 2024; Cruz-Granados et al., 2025).

The artificial endolymph formulation consisted primarily of potassium chloride (KCl; 140 mM) and potassium bicarbonate ($KHCO_3$; 25 mM), providing a potassium-rich ionic environment intended to reproduce selected features of the extracellular conditions associated with cochlear endolymph and its regulation by the stria vascularis and spiral ligament fibrocytes (Wangemann, 2006). This experimental strategy enabled comparison between standard plasma-driven culture conditions and cultures exposed to an altered ionic environment. The resulting changes in cellular organisation and immunofluorescence marker distribution were subsequently evaluated to determine whether the patient-associated cellular phenotype was modifiable following ionic supplementation.

Under standard PITTRep conditions, cultures derived from the proband and affected sibling demonstrated distinct cellular phenotypes compared with the parental cultures (Figure 1D). Reduced Stargazin (CACNG2) immunoreactivity was observed in the affected cultures, consistent with the established role of Stargazin as an AMPA receptor auxiliary subunit involved in excitatory synaptic transmission and receptor trafficking (Vandenberghe et al., 2005; Gouveia et al., 2024). In parallel, increased α-SMA immunoreactivity and differences in cellular organisation were observed in the affected cultures. These cultures exhibited fragmented and less organised cellular structures compared with the more integrated morphology observed in the parental cultures. Within the ATN framework established in the PITTRep platform, the affected cultures also showed reduced progression toward the neuron-like phenotype observed in the parental cultures, with greater persistence of adipocyte-like cellular features (Sharma et al., 2022a; Arora et al., 2025).

In contrast, parental cultures demonstrated more prominent Stargazin immunoreactivity together with comparatively organized cellular architecture and greater representation of neuron-like cellular features. These observations were consistent with the more advanced progression along the ATN-associated




FIGURE 1
(Continued).

cellular trajectory previously described for the PITTRep platform.

Following supplementation with artificial endolymph, changes in cellular organization and immunofluorescence patterns were observed in the affected cultures. Under the potassium-rich ionic condition, Stargazin immunoreactivity was more prominent and the cellular architecture appeared more cohesive compared with the corresponding cultures maintained under standard PITTRep conditions. Changes in α-SMA immunoreactivity were also observed following ionic supplementation. Similar directional changes were observed in cultures derived from both affected siblings, providing a

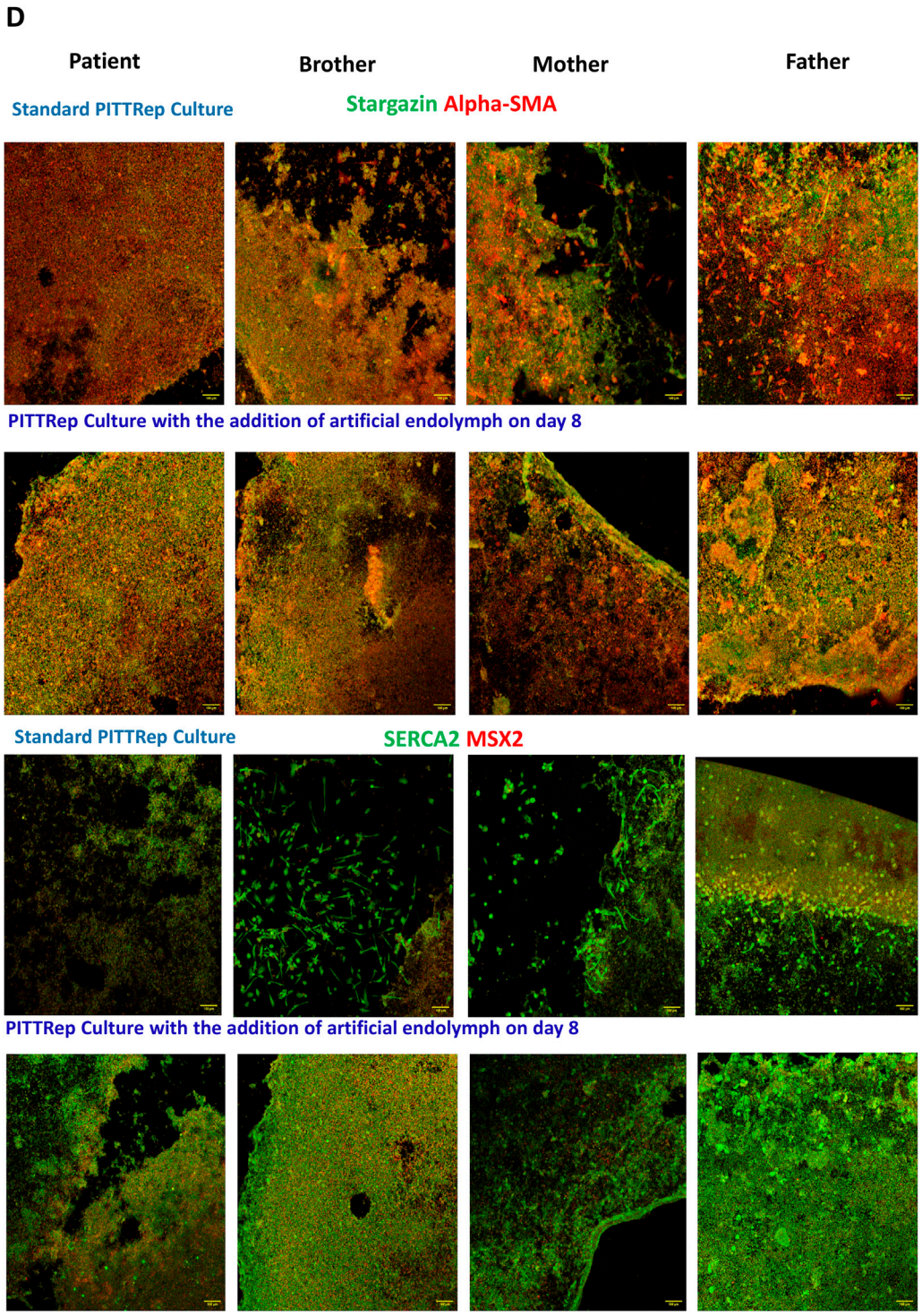


FIGURE 1
(Continued). Integrated genetic and functional analysis of familial SNHL associated with a POU3F4 variant and microenvironment-dependent functional modulation **(A)** Family pedigree demonstrating X-linked inheritance of sensorineural hearing loss, with affected male siblings and maternal carrier status. **(B)** Whole-exome sequencing identifying a hemizygous pathogenic variant in the POU3F4 gene in the proband. **(C)** Massive parallel sequencing confirming the presence of the POU3F4 variant in both affected siblings. **(D)** Immunofluorescence-based functional assessment of PITTRep cultures under standard conditions and following artificial endolymph supplementation. Upper panels show expression of Stargazin (green) and α-SMA (red), while lower panels show SERCA2 (green) and MSX2 (red) across patient, sibling, and parental control samples. Under standard conditions, patient-derived cultures exhibit reduced neuronal marker expression, increased structural marker expression, and disrupted tissue morphology, consistent with impaired adipocyte-to-neuronal transdifferentiation (ATN). Endolymph supplementation enhances neuronal marker expression, improves tissue organization, and partially restores functional and regulatory features in affected samples, indicating microenvironment-dependent modulation.

reproducible within-family observation. These findings suggest that the patient-associated cellular phenotype captured by PITTRep can be modified by alteration of the extracellular ionic environment; however, the present data do not establish functional restoration or demonstrate reversal of the underlying POU3F4-associated defect.

Further characterization using SERCA2 (ATP2A2) and MSX2 provided additional evidence of cellular changes following artificial endolymph supplementation. SERCA2 is an important regulator of intracellular calcium homeostasis, while MSX2 is a developmental transcription factor associated with neural crest development, epithelial–mesenchymal interactions, and sensory organ morphogenesis (Satokata et al., 2000; Keuls et al., 2023; Busby et al., 2025) Following ionic supplementation, changes in SERCA2 and MSX2 immunoreactivity were observed in the affected cultures, accompanied by the changes in cellular organization described above. These findings indicate that alteration of the extracellular ionic environment was associated with changes in markers related to calcium homeostasis and developmental regulation. Although these observations are consistent with modulation of cellular state, they do not by themselves establish restoration of calcium-dependent signalling or reactivation of developmental programs.

To quantitatively assess these culture-dependent changes, immunofluorescence intensity was measured from the corresponding images and analysed across four matched donor observations. In this exploratory paired analysis, artificial endolymph supplementation was associated with a significant reduction in α-SMA fluorescence ($p$ = 0.022) and a significant increase in SERCA2 fluorescence ($p$ = 0.007), whereas Stargazin ($p$ = 0.595) and MSX2 ($p$ = 0.117) did not show statistically significant differences between the two culture conditions. Fluorescence intensity within the corresponding α-SMA–Stargazin and SERCA2–MSX2 co-expressing regions was also quantitatively assessed, with the results shown in Supplementary Figures S1 and S2. Quantitative donor-level measurements and within-donor normalised values are provided in Supplementary Figures S1 and S2."

Collectively, this case demonstrates the feasibility of using patient-specific PITTRep cultures to examine cellular phenotypes associated with a genetically defined form of hereditary hearing loss and to investigate their response to an altered ionic microenvironment. The combination of patient-derived culture, cellular marker characterization, and artificial endolymph supplementation provides a proof-of-concept framework for examining genotype–phenotype relationships under controlled environmental conditions. Although these findings do not establish therapeutic efficacy or reversal of the underlying POU3F4-associated defect, they demonstrate the potential of patient-specific PITTRep cultures as a complementary experimental system for investigating cellular responses that cannot be inferred from genomic information alone. Further studies involving larger cohorts, quantitative molecular and cellular analyses, and direct functional assays will be required to determine the reproducibility and biological significance of these observations.

## Patient-specific neurovascular modeling reveals regulatory remodelling and impaired adipocyte-to-neuronal transition in MYO7A-associated sensorineural hearing loss

### Case study II: bilateral congenital severe sensorineural hearing loss associated with a MYO7A variant

To investigate whether patient-specific genomic variants influence the adipocyte-to-neurogenic transdifferentiation (ATN) continuum, we evaluated a child with congenital bilateral severe sensorineural hearing loss (SNHL) using an integrated genomic and functional modelling strategy. The proband, a 3-year-old female, presented with absent auditory responsiveness since infancy, which was confirmed by brainstem evoked response audiometry (BERA), demonstrating profound bilateral hearing impairment (Figure 2A). Antenatal and perinatal histories were uneventful, with a full-term normal delivery, excluding major prenatal environmental insults. However, developmental assessment revealed delayed motor milestones, suggesting that the disorder extended beyond isolated cochlear dysfunction. Although no family history of hearing loss was identified, the patient's father exhibited severe nystagmus, raising the possibility of an underlying hereditary neurodevelopmental predisposition. Owing to the severity of hearing impairment, the patient subsequently underwent bilateral cochlear implantation.

Ophthalmological evaluation was also performed to assess possible extra-auditory manifestations associated with the MYO7A phenotype. Fundus examination demonstrated 360° peripheral retinal pigment epithelium (RPE) loss, while fundus autofluorescence imaging showed a central area of increased autofluorescence (Figures 2N,O). These findings provided additional evidence of retinal involvement in the patient and were considered alongside the auditory and molecular findings in the clinical characterization of the case.

To establish the molecular basis of the disease, whole-exome sequencing (WES) was performed followed by Sanger validation and clinical whole-genome sequencing (WGS) (Figures 2B–E). Pedigree analysis suggested an autosomal recessive mode of inheritance (Figure 2A), while WES identified a homozygous MYO7A variant (c.5498G>A; p. Gly1833Asp), which was subsequently confirmed by Sanger sequencing (Figure 2C). Clinical WGS further detected additional variants of uncertain significance (VUSs) in tectorin alpha (TECTA) and lipoxygenase homology domains 1 (LOXHD1), both of which are well-established deafness-associated genes (Verhoeven et al., 1998; Grillet et al., 2009). Nevertheless, despite comprehensive genomic characterization, the identified variants could not be functionally prioritised, and the MYO7A alteration remained classified as a Variant of Uncertain Significance (VUS), highlighting the persistent disconnect between genomic diagnosis and biological interpretation (Richards et al., 2015a).

This limitation is particularly relevant in hereditary hearing loss because the presence of a pathogenic or potentially pathogenic variant does not necessarily predict

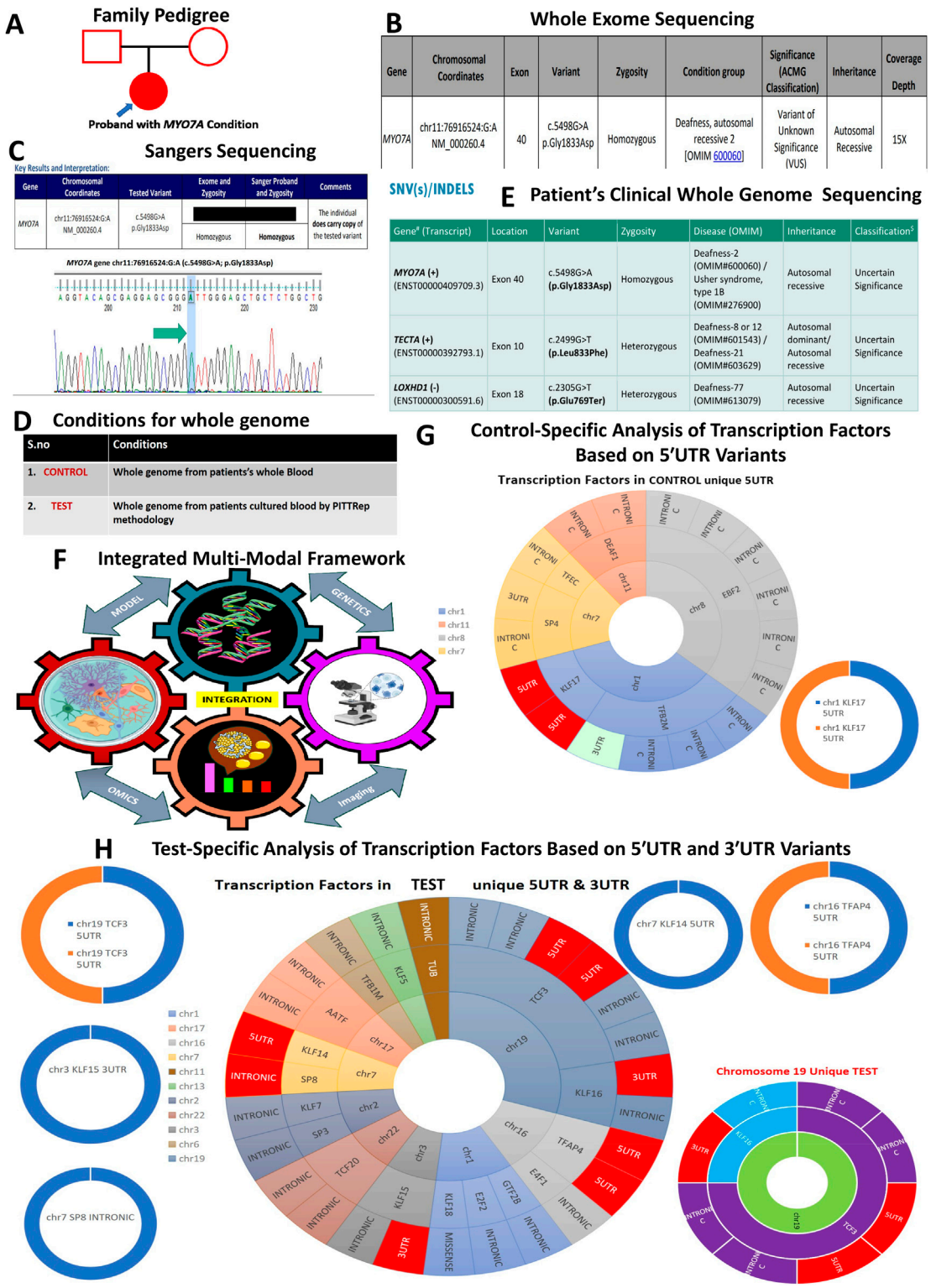


FIGURE 2
(Continued).

disease severity or functional outcome. MYO7A encodes an unconventional actin-based motor protein that is indispensable for stereocilia organization, intracellular cargo transport, mechanotransduction, and maintenance of cochlear hair-cell architecture (Verhoeven et al., 1998; Richards et al., 2015a; 2015b; Harrison et al., 2019). However, patients harboring




FIGURE 2
(Continued).

identical or closely related MYO7A variants frequently exhibit substantial variability in hearing thresholds, vestibular dysfunction, neurodevelopmental adaptation, cochlear implant responsiveness, and long-term auditory rehabilitation (Eshraghi et al., 2020; Kim and Choi, 2022; Han et al., 2024) Such phenotypic heterogeneity indicates that the coding mutation alone cannot

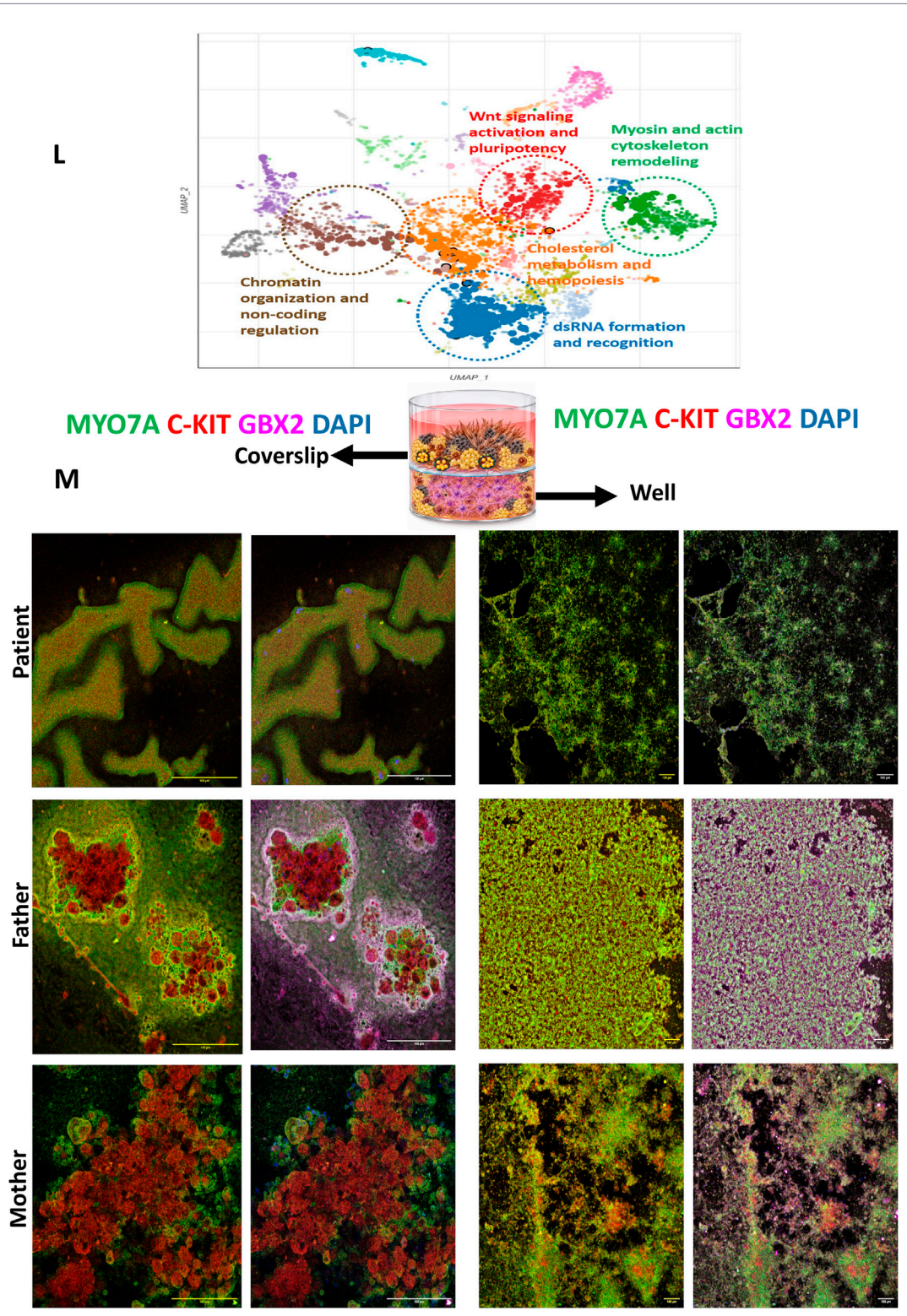


FIGURE 2
(Continued).

fully explain disease manifestation and suggests that downstream regulatory mechanisms, adaptive cellular responses, and developmental plasticity contribute significantly to the final clinical phenotype.

Although WES and WGS accurately define coding and non-coding genomic variation, both approaches provide predominantly static information regarding genomic architecture and therefore offer limited insight into the functional

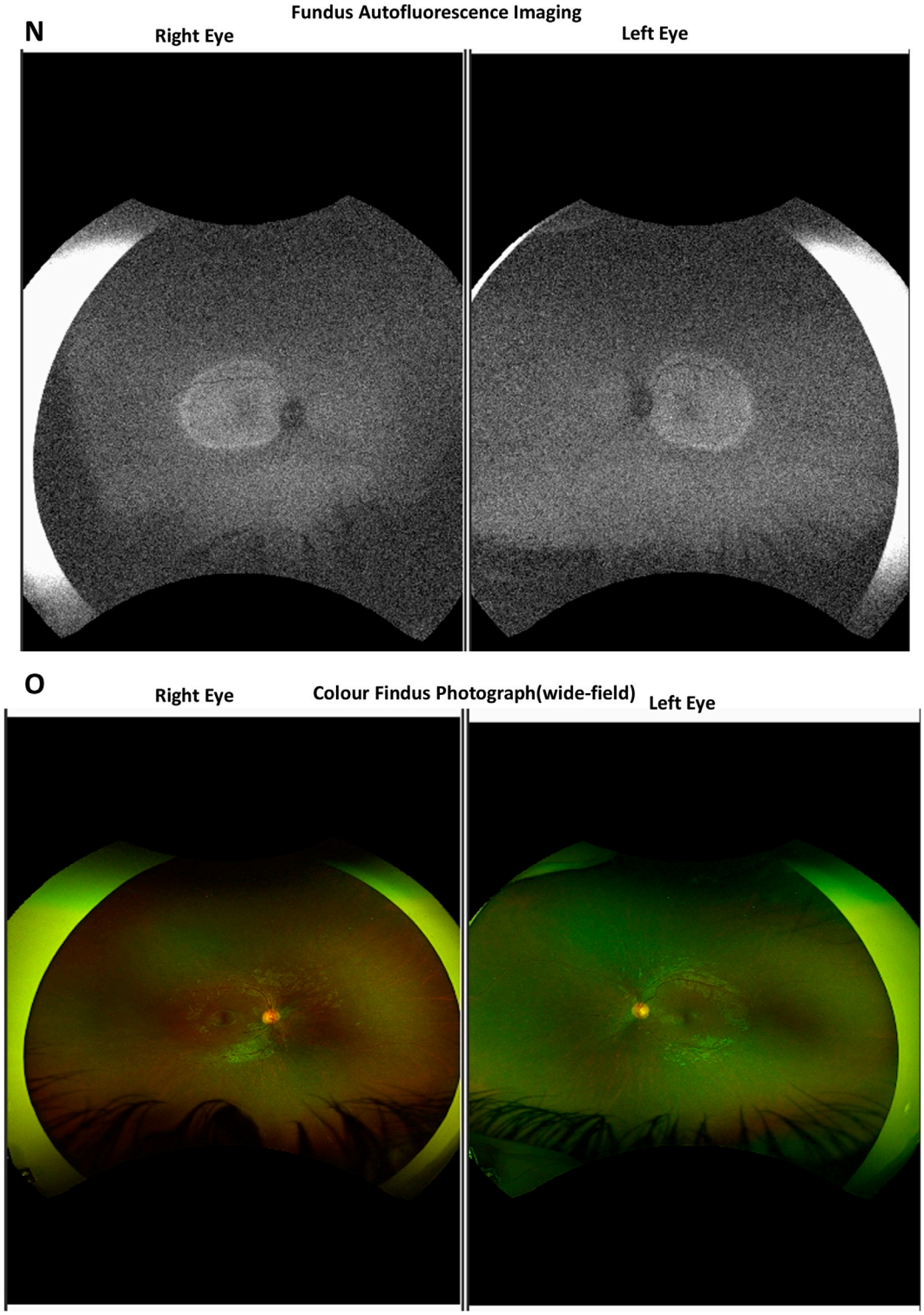


FIGURE 2
(Continued). Integrated patient-specific genomic and functional modelling of MYO7A-associated congenital sensorineural hearing loss using the PITTRep neurovascular platform Figure 2 **(A–H)**. Integrated genomic and functional characterization of patient-specific alterations in MYO7A-associated sensorineural hearing loss. **(A)** Family pedigree of the proband showing no prior history of hearing loss, indicating a non-familial presentation of sensorineural hearing loss. **(B)** Whole-exome sequencing identifying a variant in the MYO7A gene (c.5498G>A; p. Gly1833Asp), classified as a variant of uncertain significance. **(C)** Sanger sequencing chromatogram confirming the presence of the MYO7A variant in the proband. **(D)** Experimental workflow illustrating the PITTRep platform, including parallel processing of neat whole blood (control) and patient-derived plasma-induced culture (test), followed by whole-genome sequencing and downstream analysis. **(E)** Clinical whole-genome sequencing report of the control (whole blood) sample confirming the MYO7A variant without significant regulatory alterations. **(F)** Conceptual framework of the integrated diagnostic pipeline combining genomic analysis, patient-specific culture, multi-omics profiling, and functional interpretation to assess variant-associated effects. **(G)** Genomic and regulatory analysis of the control sample showing predominance of intronic variants and limited

*(Continued)*

FIGURE 2 (Continued)
5′UTR-associated changes in transcription factors, consistent with a baseline transcriptional state and absence of active regulatory reprogramming. **(H)** Genomic and regulatory analysis of the patient-derived culture sample demonstrating enrichment of 5′UTR and 3′UTR variants in transcription factors (including transcription factor AP-4 (TFAP4), transcription factor 3 (TCF3), Kruppel-like factor 14 (KLF14), Kruppel-like factor 15 (KLF15), and specificity protein 8 (SP8)), indicating culture-induced regulatory activation and patient-specific transcriptional reprogramming. **(I)** Analysis of long non-coding RNAs (lncRNAs) associated with transcription factors harboring unique 5′UTR and 3′UTR variants in the patient-derived culture. Shared lncRNA signatures, including LINC00618, indicate coordinated regulation of transcriptional activity under culture-induced stress conditions. **(J)** Pathway enrichment analysis (Enrichr/WikiPathways) of transcription factors with UTR-associated variants, demonstrating activation of pathways related to Wnt signaling, neurogenesis, olfactory epithelium regulation, adipogenesis, and chromatin organization, indicating a coordinated regulatory network. **(K–L)** UMAP-based dimensionality reduction showing clustering of transcriptional and regulatory features within the PITTRep culture system. Distinct clusters correspond to chromatin organization, non-coding RNA regulation, Wnt signaling, and lineage differentiation, indicating structured regulatory domains. **(M)** Comparative immunofluorescence analysis of adipocyte-to-neuronal transdifferentiation (ATN) across patient and parental controls under two spatial microenvironments: coverslip regions (normoxia condition) and well regions (hypoxia-like conditions) Staining for MYO7A (green), c-KIT (red), GBX2 (magenta), and DAPI (blue) demonstrates efficient lineage transition in control samples, with robust GBX2 expression and organized neuronal features, particularly enhanced under coverslip conditions. In contrast, patient-derived cultures exhibit markedly reduced or absent GBX2 expression in both coverslip and well regions, with predominant adipocytic phenotypes and limited evidence of neuronal differentiation. These findings indicate impaired ATN and disrupted lineage progression in the patient, despite microenvironmental cues that promote neuronal differentiation in controls. **(N)** Fundus autofluorescence imaging demonstrating a central area of increased autofluorescence with peripheral areas of reduced autofluorescence corresponding to retinal pigment epithelium (RPE) loss. **(O)** Color fundus photographs demonstrating extensive peripheral retinal pigment epithelium (RPE) loss/atrophy in both eyes.

consequences of identified variants (Eshraghi et al., 2020; Kim and Choi, 2022) Importantly, sequencing cannot determine whether a mutation alters transcriptional regulation, epigenetic remodelling, mitochondrial adaptation, neuronal differentiation, or lineage plasticity. Likewise, restoration of hearing following cochlear implantation depends not only on preservation of cochlear hair cells but also on the integrity of spiral ganglion neurons, central auditory circuitry, neurovascular support, and activity-dependent neuronal remodelling (Thulasiram et al., 2022; Larsen et al., 2025) Consequently, patients carrying similar genomic variants often demonstrate markedly different clinical outcomes despite comparable genetic findings, emphasizing the need for functional systems capable of translating static genomic information into dynamic biological phenotypes.

Building upon our previous demonstration that the Plasma-Induced Transcriptomic and Epitranscriptomic Reprogramming (PITTRep) platform reproducibly supports adipocyte-to-neurogenic transdifferentiation through endogenous plasma-derived regulatory programs (Arora et al., 2025; Sharma et al., 2022a), we hypothesized that unresolved genomic variation might be associated with altered progression through this cellular continuum. Rather than examining the MYO7A variant as an isolated coding alteration, we sought to determine whether patient-specific cellular and regulatory differences were associated with changes in the coordinated processes underlying adipogenic remodelling, neuronal lineage-associated features, and neurovascular organization. To address this, autologous blood from the patient was subjected to PITTRep-mediated cellular remodelling and compared with the corresponding baseline whole-blood sample, enabling assessment of genomic features together with cellular and lineage-associated changes within an integrated multimodal framework (Figure 2F). This approach provided a basis for examining whether patient-specific cellular remodelling could reveal phenotypic differences along the adipocyte-to-neurogenic transdifferentiation continuum that are not apparent from genomic analysis alone.

## Plasma-induced cellular remodelling reveals patient-specific regulatory adaptation beyond the MYO7A coding variant

To determine whether the identified genomic variants were associated with patient-specific cellular and regulatory changes, autologous blood from the patient was subjected to the Plasma-Induced Transcriptomic and Epitranscriptomic Reprogramming (PITTRep) platform, while neat whole blood served as the baseline genomic reference (Figure 2F). Unlike conventional sequencing approaches, which primarily characterise the genomic sequence, the PITTRep system provides a plasma-based microenvironment containing endogenous cytokines, extracellular vesicles, inflammatory mediators, growth factors, and metabolic regulators, thereby enabling examination of patient-derived cells under dynamic culture conditions (Sharma et al., 2022a; Yáñez-Mó et al., 2015). This experimental framework enabled comparison of the baseline genomic state with cellular changes observed following plasma-induced remodelling, providing an approach to investigate patient-specific regulatory and lineage-associated phenotypes beyond the coding variant itself.

Comparative whole-genome analysis revealed that the original MYO7A coding variant remained completely stable following plasma-induced culture, indicating that the observed biological responses were not attributable to modification of the underlying pathogenic mutation. Instead, the cultured system demonstrated extensive context-dependent regulatory remodelling, predominantly involving untranslated (5′UTR and 3′UTR) and intronic regions of multiple transcription-associated genes (Figures 2G,H). Such regions are increasingly recognized as critical regulatory platforms governing RNA stability, translational efficiency, alternative splicing, microRNA binding, chromatin organization, and higher-order transcriptional control (Statello et al., 2021a; Jafari-Raddani et al., 2022). The predominance of differences within regulatory rather than coding regions was therefore consistent with the possibility that plasma-induced cellular

remodelling was accompanied by changes in regulatory programs beyond the primary MYO7A coding variant.

Among the most prominent regulatory changes was the emergence of transcription factors associated with developmental plasticity and lineage specification, including TFAP4, TCF3, KLF14, KLF15, and SP8, which were selectively enriched following plasma-induced remodelling. Several of these transcription factors exhibited unique 5′UTR- and 3′UTR-associated variants that were absent in baseline whole blood, suggesting activation of context-dependent regulatory programs rather than constitutive genomic variation. Because these transcription factors regulate cellular differentiation, metabolic adaptation, stem-cell maintenance, and developmental commitment (Flitsch et al., 2020; Davies et al., 2023; Du and Wang, 2025) their representation in the post-remodelling profile provides candidate regulatory features that may be relevant to the altered cellular phenotype and ATN-associated remodelling observed in the patient-derived culture.

Network analysis further demonstrated that these transcription factors were associated with common long non-coding RNA (lncRNA)-related regulatory modules, with LINC00618 occupying a prominent position within the identified network (Figure 2I). These associations suggested convergence of multiple transcription-factor-related features within a non-coding RNA regulatory network rather than independent representation of individual transcription factors. Such lncRNA-associated regulatory networks have previously been implicated in chromatin organization, stress adaptation, and developmental gene regulation (Statello et al., 2021b; Segal and Dostie, 2023). The identification of untranslated regulatory regions together with lncRNA-associated interactions therefore provides evidence for a broader regulatory layer accompanying plasma-induced cellular remodelling and raises the possibility that non-coding regulatory mechanisms contribute to the ATN-associated phenotype observed in the patient-derived culture.

Importantly, because the identified MYO7A variant resides on chromosome 11q13.5, these observations could be interpreted within the chromosome 11 sensory-developmental regulatory framework established in our previous PITTRep study. In that work, chromosome 11 emerged as a transcriptionally active developmental hub integrating olfactory signalling, developmental hemoglobin switching, and extensive non-coding regulatory remodelling during plasma-induced reprogramming (Sharma et al., 2022a) Consistent with these earlier observations, the present patient exhibited widespread remodelling of untranslated and intronic regulatory regions while the MYO7A coding mutation remained unchanged. These findings raise the possibility that chromosome 11-associated regulatory features may contribute to the cellular and ATN-associated phenotype observed in the present case, although a direct mechanistic relationship between these regulatory features and the MYO7A variant cannot be established from the current data.

To determine whether these regulatory adaptations translated into coordinated biological programs, pathway enrichment and transcriptional clustering analyses were subsequently performed.

## Regulatory remodelling converges on developmental signalling networks associated with cellular plasticity

To determine whether the observed regulatory features were associated with coordinated biological processes rather than representing isolated genomic findings, pathway enrichment analysis was performed using Enrichr, WikiPathways, and Reactome databases (Figure 2J). Consistent with the transcription-factor-associated features identified following plasma induction, pathway analysis demonstrated enrichment of developmental and cellular regulatory pathways, including Wnt/β-catenin signalling, olfactory transduction, ectodermal differentiation, adipogenesis, neuronal development, and stem-cell-associated pathways. These pathways are broadly involved in processes related to cellular plasticity, lineage specification, and developmental state transitions (Nusse and Clevers, 2017; Liu et al., 2022; Hu et al., 2024). Their enrichment in the patient-derived remodelling profile therefore provides candidate biological processes that may be relevant to the altered ATN-associated cellular phenotype observed in the PITTRep cultures.

Among the enriched pathways, Wnt signalling emerged as one of the predominant regulatory networks. Wnt signalling plays important roles in stem-cell maintenance, cellular polarity, cytoskeletal organization, and neuronal differentiation, while also influencing adipogenic commitment during developmental transitions (Nusse and Clevers, 2017; Liu et al., 2022; Hu et al., 2024).

The concurrent enrichment of adipogenic and neurogenic pathways was consistent with the presence of cellular programs associated with different stages of the adipocyte-to-neurogenic transdifferentiation continuum, rather than exclusive representation of a single lineage-associated state. These findings were consistent with our previous PITTRep study, in which Wnt-associated signalling was identified among the regulatory pathways associated with plasma-mediated cellular remodelling (Sharma et al., 2022b). Together, these observations suggest that Wnt-associated regulatory processes may contribute to the cellular plasticity underlying the ATN-associated phenotype observed in the present patient-derived cultures.

Interestingly, olfactory signalling again emerged as one of the significantly enriched biological pathways. As demonstrated in our previous work, activation of olfactory receptor-associated networks within the PITTRep system extends beyond sensory perception and has been associated with broader developmental processes involving calcium signalling, mitochondrial adaptation, oxidative stress responses, and neuronal differentiation (Sharma et al., 2022b). Similar non-olfactory functions of olfactory receptors have been reported in multiple tissues, where they participate in processes including cell migration, metabolism, inflammation, and tissue regeneration (Flegel et al., 2013; Maßberg and Hatt, 2018) The enrichment of olfactory-associated signalling in the present patient therefore provides further evidence for representation of sensory-developmental regulatory pathways during plasma-induced remodelling and raises the possibility that these pathways contribute to the lineage plasticity observed within the ATN-associated cellular phenotype.

Additional enrichment of chromatin organization, RNA processing, and non-coding RNA-associated pathways further supported the representation of regulatory processes accompanying the untranslated-region findings observed following plasma induction. Collectively, these findings suggest that plasma-induced cellular remodelling is associated with multiple interconnected regulatory processes involving developmental signalling, chromatin organization, RNA processing, and non-coding RNA regulation rather than isolated gene-specific features (Statello et al., 2021b; Segal and Dostie, 2023). The convergence of these pathways provides a potential regulatory framework linking the transcription-factor-associated features identified in the patient-derived culture with biological processes relevant to adipocyte-to-neurogenic transdifferentiation.

To further examine the relationships among the enriched pathways, dimensionality reduction was performed using Uniform Manifold Approximation and Projection (UMAP) analysis (Figures 2K,L). UMAP demonstrated structured clustering of pathways associated with chromatin organization, non-coding RNA regulation, Wnt signalling, developmental differentiation, myosin-associated cytoskeletal remodelling, and neuronal specification. The spatial organization of these pathway-associated features indicated that the identified regulatory processes were not randomly distributed within the analysed dataset and showed relationships across developmental, regulatory, and lineage-associated categories.

Importantly, the proximity of developmental signalling pathways to chromatin-remodelling and lineage-specification categories was consistent with interconnected regulatory processes within the PITTRep-associated profile. These pathway relationships provide a framework for interpreting the transcription-factor and regulatory-region findings described above and suggest that the identified molecular features may be relevant to the cellular plasticity and ATN-associated phenotype observed in the patient-derived cultures. We therefore next investigated whether these molecular differences were accompanied by altered cellular morphology and lineage-associated features in patient-derived cultures compared with healthy controls.

## Patient-specific cellular remodelling reveals disruption of the adipocyte-to-neurogenic transdifferentiation continuum

Having established that plasma-induced cultures underwent coordinated regulatory remodelling involving chromosome 11-associated developmental programs, we next investigated whether these molecular adaptations translated into functional differences in cellular behavior. Because adipocyte-to-neurogenic transdifferentiation (ATN) represents the principal biological output of the PITTRep platform, patient-derived cultures were compared directly with parental healthy controls cultured under identical plasma-induced conditions (Figure 2M) (Sharma et al., 2022b; Arora et al., 2025).

As consistently observed in our previous PITTRep studies, cultures established from the parents exhibited a highly ordered developmental progression beginning with robust adipogenic expansion. During the early stages of culture, cells organized into large, early thermogenic adipocyte-rich colonies that progressively underwent structural remodelling, generating an extensive cellular niche associated with subsequent lineage transition. Rather than remaining terminally differentiated adipocytes, these enlarged cellular aggregates gradually acquired elongated cellular morphology accompanied by progressive neurite extension, ultimately forming interconnected neuron-like networks distributed throughout the culture. This sequential progression from adipogenic expansion through cellular remodelling and neuronal differentiation is consistent with the adipocyte-to-neurogenic transdifferentiation continuum previously established within the PITTRep platform (Sharma et al., 2022b; Arora et al., 2025).

In contrast, cultures established from the MYO7A-associated SNHL patient demonstrated a distinct cellular trajectory despite being maintained under identical plasma-driven conditions. Instead of forming the large, organized adipogenic colonies observed in the parental cultures, the majority of cells remained confined to small, compact cellular aggregates with limited expansion and structural remodelling. Although cellular activation was evident, these aggregates showed limited progression toward the extensive adipogenic architecture observed in the parental cultures. This altered early-stage remodelling was accompanied by reduced progression toward the subsequent cellular organization associated with the ATN continuum.

The difference became more apparent during later stages of culture. Whereas parental control cultures generated abundant elongated neuron-like cells with extensive neuritic projections that interconnected to form organized neuronal networks, patient-derived cultures exhibited sparse neuron-like cells with markedly shorter and less developed neurites. The limited neuritic processes that emerged remained largely isolated and did not form the complex intercellular networks observed in the parental cultures. Together, these observations demonstrate an altered progression through the adipocyte-to-neurogenic transdifferentiation continuum in the patient-derived culture, with differences evident at both the adipogenic-remodelling and subsequent neuronal stages.

This altered developmental progression was further examined by immunofluorescence analysis. Parental cultures demonstrated robust expression of GBX2, MYO7A, and c-KIT, consistent with representation of developmental programs associated with hindbrain specification, sensory-neuronal differentiation, and progenitor-associated cellular states (Weil et al., 1995; Richardson et al., 2011; Lennartsson and Rönnstrand, 2012). In contrast, patient-derived cultures exhibited visibly reduced expression of all three markers. Together with the altered morphological phenotype, these findings were consistent with reduced representation of developmental and neurogenic features along the ATN-associated cellular trajectory.

To complement the qualitative immunofluorescence findings, mean fluorescence intensity was quantitatively assessed for MYO7A, C-KIT, and GBX2 under coverslip and well-associated culture conditions. Quantitative measurements were also obtained from the corresponding MYO7A–C-KIT and MYO7A–C-KIT–GBX2 co-expressing regions (Supplementary Figure S3).

Importantly, these phenotypic observations were concordant with the regulatory analyses described above. Although the underlying

MYO7A coding variant remained unchanged throughout plasma-induced culture, the patient-derived profile showed differences involving untranslated and intronic regulatory regions, developmental transcription-factor-associated features, non-coding RNA networks, and chromosome 11-associated signalling pathways. The concordance between these molecular features and the altered cellular phenotype raises the possibility that regulatory processes beyond the primary MYO7A coding variant contribute to the patient-specific ATN-associated phenotype. However, the present data do not establish a direct causal relationship between the identified regulatory features and the cellular phenotype.

Clinically, this observation is notable because the patient demonstrated measurable improvement following cochlear implantation despite persistent differences in ATN-associated cellular remodelling within the PITTRep system. This distinction suggests that clinical auditory outcome and the cellular phenotype captured by PITTRep may represent related but non-equivalent dimensions of disease biology. Thus, the PITTRep phenotype may provide additional information regarding patient-specific cellular remodelling that is not captured by genomic analysis or routine clinical assessment (Richards et al., 2015a; Oza et al., 2018) Collectively, the findings from this case identify altered adipocyte-to-neurogenic transdifferentiation as a prominent cellular phenotype associated with the patient-derived MYO7A-associated SNHL culture and provide a basis for further investigation of the relationship between chromosome 11-associated regulatory features and ATN-associated cellular remodelling.

## Case Study III: systems-level dissection of ototoxicity-associated neuroinflammatory and Neurogenic Dysfunction in the absence of detectable genetic variants

A 6-year-old male presented with postlingual bilateral severe sensorineural hearing loss (SNHL), with progressive hearing impairment developing after 3 years of age following a prolonged period of critical illness. The patient had a clinically significant history of drug-induced ototoxicity associated with intensive medical management, including haemodialysis, gastrointestinal bleeding, prolonged ventilatory support requiring tracheostomy, and multisystem complications. Following recovery from the acute illness, the patient exhibited progressive hearing loss accompanied by speech regression and delayed neurodevelopmental progression, suggesting that the pathological effects extended beyond the cochlea to involve broader auditory-neural dysfunction (Waissbluth and Daniel, 2013; Ganesan et al., 2018).

Unlike the hereditary sensorineural hearing loss (SNHL) cases described previously, whole-exome sequencing did not identify a pathogenic or likely pathogenic variant associated with the patient's phenotype (Figures 3A,B). Together with the clinical history of drug-associated ototoxic exposure, the findings were considered consistent with an acquired etiology rather than an identifiable monogenic cause. This provided an opportunity to determine whether alterations in the adipocyte-to-neurogenic transdifferentiation (ATN) continuum could also be observed in SNHL without an identified disease-associated genetic variant. Patient-derived blood cells were therefore subjected to the PITTRep platform and compared directly with parental control cultures under identical plasma-induced conditions, including both the coverslip-associated normoxic microenvironment and the under coverslip well region (hypoxia associated) (Figure 3C) (Sharma et al., 2022b; Arora et al., 2025).

Within the PITTRep system, healthy parental cultures consistently followed the characteristic adipocyte-to-neurogenic transdifferentiation continuum established in our previous studies (Sharma et al., 2022b; Arora et al., 2025). During the initial stages of culture, peripheral blood-derived cells underwent extensive adipogenic remodelling, producing large adipocyte-rich cellular aggregates that subsequently underwent progressive structural reorganization, cellular elongation, and acquisition of neuron-like morphology. This transition was accompanied by neurite initiation and extension, with interconnected neuron-like networks becoming evident at later stages of culture. Consistent with this phenotype, VGLUT2, BDNF, and TRKB-associated staining was readily detectable in parental cultures, supporting the presence of neuronal and neurotrophic phenotypes (Park and Poo, 2012; Chuang et al., 2021; Antonijevic et al., 2024). Together, these observations were consistent with the characteristic adipocyte-to-neurogenic remodelling trajectory previously described for the PITTRep platform.

In contrast, patient-derived cultures demonstrated marked disruption of this developmental sequence. Rather than undergoing the progressive adipogenic expansion observed in parental controls, cells remained predominantly confined to small, compact aggregates with limited hypertrophy and reduced structural organization under both coverslip and well conditions. Although cellular activation and remodelling were evident, these aggregates did not develop into the larger adipocyte-rich structures observed in healthy controls, suggesting an interruption of lineage progression at an early stage of the ATN continuum. At later stages, only a limited number of neuron-like cells were observed, with relatively thin and shortened neuritic projections and limited network formation compared with parental cultures. Together, these findings indicate that patient-derived cultures exhibited altered progression from adipogenic remodelling toward neurogenic differentiation, suggesting that the cellular consequences associated with the patient's ototoxicity history extend beyond the appearance of mature neuronal phenotypes to earlier stages of the ATN-associated remodelling trajectory.

The impaired neuronal phenotype was further supported by reduced expression of VGLUT2, BDNF, and TRKB throughout the patient-derived cultures. VGLUT2 is associated with glutamatergic neurotransmission and excitatory neuronal differentiation, whereas the BDNF–TRKB signalling axis is involved in neuronal survival, axonal growth, synaptic stabilization, and activity-dependent plasticity (Park and Poo, 2012; Chuang et al., 2021; Antonijevic et al., 2024). The concurrent reduction of these neuronal and neurotrophic markers was consistent with reduced representation of neuronal differentiation and neurotrophic signalling features within the patient-derived cultures. In contrast, both parental cultures demonstrated robust expression of these markers, consistent with preservation of neuronal and neurotrophic features associated with progression through the ATN continuum.

Interestingly, the well-associated hypoxic microenvironment, which has previously been observed to enhance adipogenic

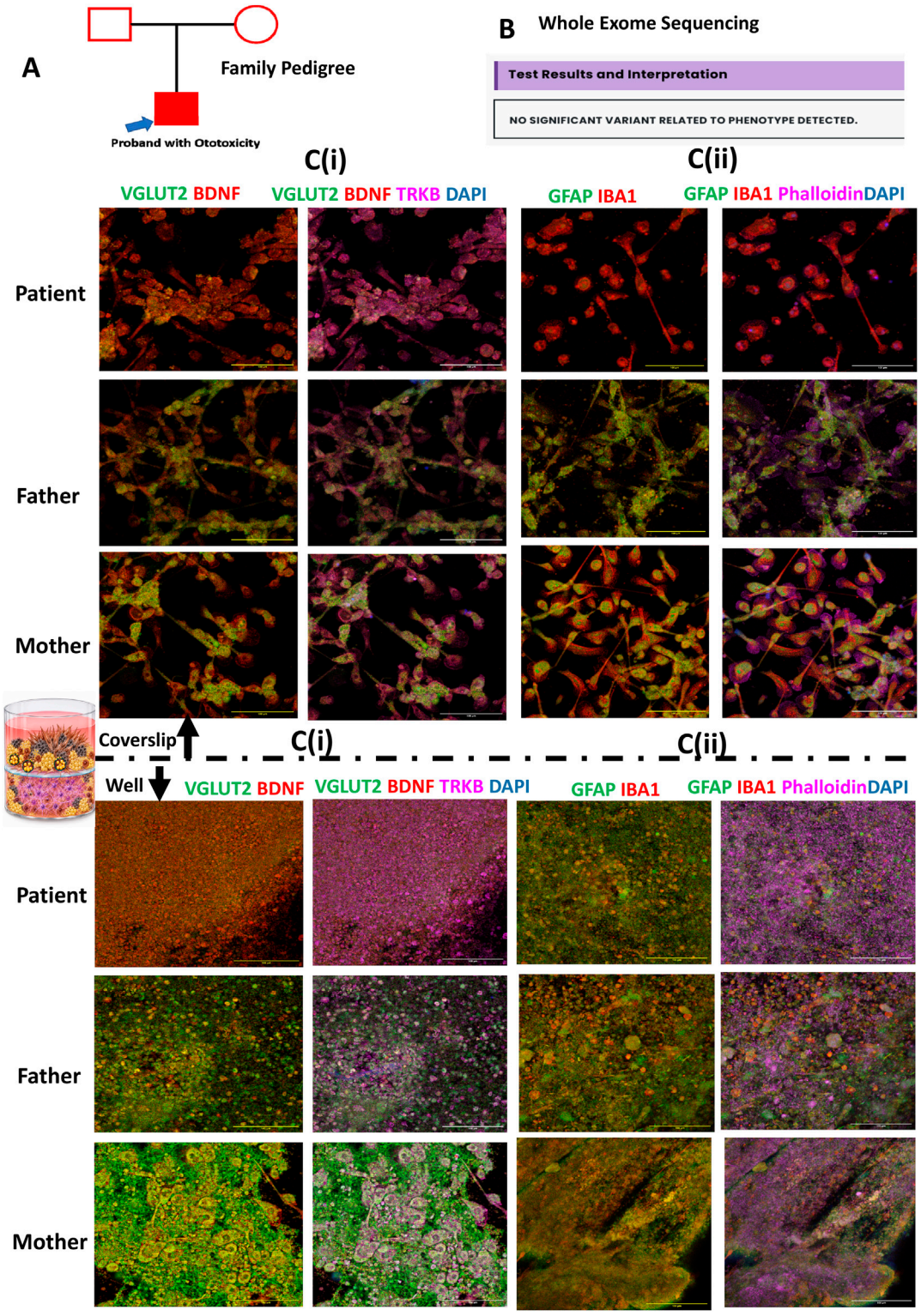


FIGURE 3
Patient-Specific Neuroinflammatory and Neurogenic Dysfunction in Ototoxicity-Associated Sensorineural Hearing Loss Without Detectable Genetic Variants **(A)** Family pedigree of a patient with postlingual bilateral severe sensorineural hearing loss (SNHL) associated with ototoxic injury. No familial history of hearing loss was identified. **(B)** Whole-exome sequencing demonstrating absence of pathogenic or likely pathogenic variants associated with the auditory phenotype, indicating a genetically unresolved case. **(C-i)** Immunofluorescence-based analysis of neuronal differentiation and synaptic-associated markers in coverslip-associated normoxic microenvironment and standard well conditions (hypoxic) within the PITTRep platform. Patient-derived cultures demonstrated markedly reduced expression of VGLUT2 together with altered BDNF and TRKB expression compared with parental controls, indicating impaired glutamatergic neuronal differentiation and defective synaptic-associated signaling. **(C-ii)** Immunofluorescence analysis of neuroglial and inflammatory markers including GFAP, IBA1, and Phalloidin. Patient-derived cultures demonstrated elevated IBA1 expression, reduced GFAP expression, and disrupted cytoskeletal organization, suggesting persistent neuroinflammatory activation, impaired astroglial support, and structural dysregulation following ototoxic injury.

remodelling and neuronal differentiation within healthy PITTRep cultures (Sharma et al., 2022b; Arora et al., 2025), did not restore the patient-derived phenotype. Despite exposure to the same endogenous plasma-derived cues and the coverslip-associated normoxic culture environment, patient-derived aggregates remained small and showed limited structural remodelling and neurite extension. The persistence of these differences in both coverslip and well conditions indicates that the altered cellular phenotype was not readily reversed by the hypoxia-associated microenvironment (well) that supported remodelling in parental cultures. These findings suggest that the patient's cellular response to the PITTRep microenvironment differs from that observed in parental controls and is associated with reduced progression through the ATN continuum. Thus, in this case, the observed phenotype extends beyond reduced neuronal marker expression and includes altered progression through earlier stages of adipogenic and neurogenic remodelling.

To determine whether the altered cellular phenotype was accompanied by changes in glial- and immune-associated cellular features, cultures were further characterised using GFAP, IBA1, and phalloidin immunostaining (Figure 3C). Patient-derived cultures exhibited pronounced IBA1-associated staining together with relatively diminished GFAP immunoreactivity, indicating an altered distribution of microglial- and astroglial-associated cellular phenotypes compared with parental controls. IBA1-positive cellular states have been associated with inflammatory and stress-responsive responses, while astroglial populations contribute to neuronal homeostasis and trophic support; persistent inflammatory signalling can adversely affect neuronal homeostasis and regenerative processes (Wang et al., 2019; Kitama et al., 2025; Li et al., 2026) The present findings therefore suggest that the altered ATN-associated phenotype occurred alongside changes in glial- and immune-associated cellular states.

To quantitatively support these observations, mean fluorescence intensity was assessed for neuronal markers (VGLUT2, BDNF, and TRKB) and glial/cytoskeletal markers (GFAP, IBA1, and Phalloidin) under coverslip and well-associated culture conditions. Fluorescence intensity within the corresponding co-expressing regions was also assessed, with quantitative measurements provided in Supplementary Figures S4 and S5.

Concurrently, phalloidin staining demonstrated marked differences in filamentous actin organization, with less organized cytoskeletal architecture and reduced cellular polarization compared with the more organized actin networks observed in parental controls. Because cytoskeletal remodelling contributes to cellular elongation, neurite extension, intracellular trafficking, and neuronal polarization (Brown and Macklin, 2020; Hilton et al., 2024). The observed cytoskeletal differences are consistent with the reduced cellular remodelling and neurite development observed in the patient-derived cultures.

Importantly, these findings support the interpretation that adipocyte-to-neurogenic transdifferentiation is not defined solely by the appearance of neuron-like cells but involves a sequential cellular remodelling process encompassing adipogenic expansion, cellular hypertrophy, intermediate structural remodelling, neurite initiation, neuronal differentiation, and subsequent network formation. In the present case, differences were evident at multiple stages of this trajectory, beginning with limited adipogenic expansion and remodelling and extending to reduced neurite development and network formation. Thus, the observed phenotype represents an alteration of the broader ATN-associated cellular trajectory rather than an isolated reduction in neuronal differentiation.

Collectively, this case demonstrates that patient-specific alterations in ATN-associated cellular remodelling can be observed in an acquired form of SNHL in which no significant phenotype-associated variant was identified by WES. The patient-derived phenotype was accompanied by altered neuronal and neurotrophic marker expression, IBA1/GFAP-associated cellular features, and cytoskeletal organization. These findings indicate that the cellular phenotype captured by PITTRep is not necessarily dependent on identification of a monogenic cause and may reflect convergent effects of different disease contexts on cellular remodelling. However, the present case does not establish that neuroinflammation, impaired neurotrophic signalling, or cytoskeletal disorganization independently caused the ATN phenotype. Rather, these features provide candidate biological processes for further investigation. Together with the genetically characterised cases, the findings support the potential utility of PITTRep as a patient-specific functional model for examining cellular phenotypes that may not be apparent from genomic analysis alone.

## GJB2 genotype–phenotype characterization

GJB2, encoding connexin 26 (Cx26), is a well-established cause of hereditary sensorineural hearing loss (SNHL). Pathogenic GJB2 variants include different molecular classes, including truncating and missense variants, and are associated with variable clinical presentations (Hegde et al., 2022; Morris et al., 2026). Biallelic loss-of-function variants, such as the truncating c.71G>A; p. Trp24Ter (W24*) variant, are commonly associated with congenital or early-onset autosomal recessive nonsyndromic hearing loss, whereas c.551G>A; p. Arg184Gln missense variants may be associated with autosomal dominant hearing loss and variable phenotypic expression (Figure 4). In the present study, three patients from two families carrying distinct GJB2 variants were evaluated to examine the relationship between genotype, clinical phenotype, and patient-derived functional phenotypes using the PITTRep platform. The cases included a family with a truncating variant associated with congenital profound hearing loss and a second family with a missense variant, a positive family history, and progressive hearing loss (Su et al., 2010; Hegde et al., 2022; Morris et al., 2026).

Because our functional investigation focused specifically on adipocyte-to-neuronal transdifferentiation (ATN), we sought markers that could practically capture the cellular transition from the adipocyte-derived state toward neuronal differentiation in patient-derived cultures. In our previous study, retinoid metabolism emerged as one of the prominent molecular signatures associated with the ATN process, with ADH6 identified among the associated genes (Sharma et al., 2022a). This provided the rationale for evaluating ADH6 in the present patient-derived cultures. Retinoids are particularly relevant to the ATN model because adipose tissue represents an important extrahepatic reservoir of retinol, second only to the liver, and retinol undergoes sequential oxidation to

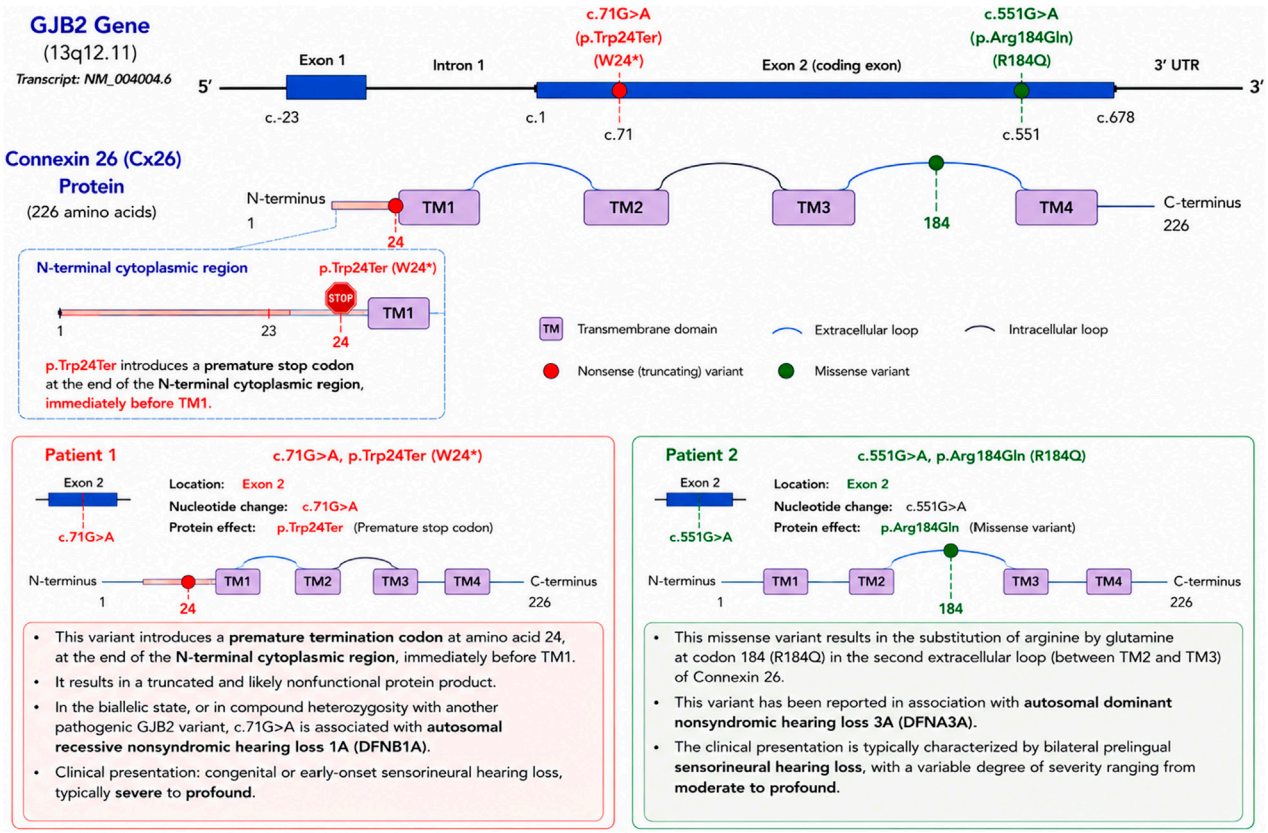


FIGURE 4
Structural mapping of pathogenic GJB2 variants associated with hereditary hearing loss. Schematic representation of the GJB2 gene and Connexin 26 (Cx26) protein architecture illustrating the pathogenic variants identified in the present study. The GJB2 gene, located on chromosome 13q11–q12, encodes the 226 amino acid gap-junction protein Connexin 26, which contains four transmembrane domains (TM1–TM4), intracellular loops, extracellular loops, and cytoplasmic N- and C-terminal regions.

retinaldehyde and subsequently retinoic acid, a signalling molecule involved in cellular differentiation and developmental processes (Kumar et al., 2012; Esposito et al., 2024; Wang and Du, 2024). We therefore investigated ADH6 as a candidate marker of the retinoid-associated metabolic state during ATN, together with SERCA2 to assess calcium-handling-associated cellular characteristics across the differentiating cultures.

The PITTRep platform generates bipotential patient-derived cells from autologous blood that can undergo differentiation toward neuro-mesodermal lineages. To describe the relative representation of these two lineage phenotypes, we used a qualitative nomenclature in which N denotes a predominant neuronal phenotype, n a lesser neuronal component, M a predominant mesodermal phenotype, and m a lesser mesodermal component. Thus, NM represents predominant neuronal and mesodermal components, Nm predominant neuronal with a minor mesodermal component, nM a minor neuronal component with predominant mesodermal features, and nm relatively minor representation of both lineages. This nomenclature was used to describe the relative cellular phenotype observed within the PITTRep cultures rather than to define discrete cell populations.

The figure highlights two clinically significant variants identified in patient-derived hereditary hearing loss cases. The first variant, c.71G>A (p.Trp24Ter; W24*), is a nonsense/truncating mutation located near the end of the N-terminal region at the beginning of TM1 (Figure 4). This variant introduces a premature termination codon at amino acid position 24, resulting in a truncated and likely nonfunctional Connexin 26 protein. The variant is a well-established cause of autosomal recessive nonsyndromic hearing loss DFNB1A and is commonly associated with congenital or early-onset severe-to-profound sensorineural hearing loss (Morris et al., 2026).

The second variant, c.551G>A (p.Arg184Gln; R184Q), is a missense mutation located within the second extracellular loop between TM2 and TM3 of Connexin 26 (Figure 4). This variant results in substitution of arginine by glutamine at codon 184 and has been associated with autosomal dominant deafness DFNA3A characterised by variable expressivity ranging from moderate to profound bilateral prelingual sensorineural hearing loss. Previous reports additionally suggest that the phenotypic spectrum may extend beyond isolated auditory dysfunction to include ectodermal manifestations such as dry skin and nail abnormalities (Su et al., 2010).

The structural localization of both variants within distinct functional domains of Connexin 26 suggests differential effects on gap-junction assembly, intercellular ionic communication, metabolic coupling, and neurovascular signalling, potentially contributing to the distinct neurovascular and

adipocytic-to-neurogenic remodelling phenotypes observed within the patient-derived PITTRep neurovascular tissue system.

## Case Study IV: disease modelling of GJB2-associated congenital sensorineural hearing loss reveals impaired neurogenic plasticity

A patient with bilateral congenital severe sensorineural hearing loss (SNHL) was identified with a homozygous pathogenic GJB2 variant [c.71G>A; p. Trp24Ter], a well-established loss-of-function mutation associated with autosomal recessive deafness type 1A (Figures 5A,B). GJB2 encodes Connexin-26, a gap-junction protein essential for potassium recycling, intercellular ionic communication, calcium-wave propagation, and metabolic coupling within the cochlea (Mammano, 2019; Hegde et al., 2022). Pathogenic variants in GJB2 are among the most common causes of hereditary congenital hearing loss worldwide and are classically associated with disruption of cochlear homeostasis, sensory-neural degeneration, and impaired auditory signalling.

However, despite definitive genomic identification of the pathogenic variant, sequencing alone remains insufficient to explain patient-specific differences in developmental plasticity, neuronal remodelling, and adaptive cellular behavior. Increasing evidence suggests that connexin-associated auditory pathology extends beyond isolated potassium dysregulation and additionally involves impaired calcium signalling, mitochondrial dysfunction, oxidative stress imbalance, altered intercellular metabolic coordination, and defective neurodevelopmental adaptation (Zhu et al., 2015; Fetoni et al., 2018; Sun et al., 2022). Consequently, functional systems-level interrogation becomes essential to understand how disruption of connexin-mediated signalling influences lineage-associated neurogenic remodelling and stress-responsive plasticity.

To investigate these mechanisms, patient-derived blood samples were subjected to the PITTRep platform under two spatial microenvironmental conditions consisting of coverslip-associated normoxic adherent regions and well-associated hypoxic/stress-responsive microenvironments (Figure 5C). Within the PITTRep system, the well microenvironment generates localized stress-associated hypoxic conditions capable of promoting adaptive transcriptional remodelling, adipocyte-to-neuronal transdifferentiation (ATN), and neuronal-network formation. This configuration therefore enabled assessment of whether hypoxia-responsive neurogenic plasticity remained functionally inducible within the GJB2-associated disease state.

In the patient-derived cultures, the overall phenotype was characterised as nM, with a relatively limited or distorted neuronal component and a predominant mesodermal phenotype. In contrast to the organized neuronal-network formation observed in parental control cultures, patient-derived cultures showed reduced neuronal representation and persistence of mesodermal characteristics, indicating incomplete progression from the adipocyte-derived state toward the neuronal phenotype. This difference was evident across the evaluated microenvironmental conditions and provided a patient-specific functional phenotype associated with the GJB2-related hearing-loss state (Morris et al., 2026).

ADH6 expression further supported this difference in ATN-associated progression. In control cultures, ADH6-positive cells were observed during the earlier/intermediate stages of neuronal remodelling, whereas ADH6 staining became less prominent with more mature neuronal differentiation, majorly showing Nm phenotype in control cultures. In the patient-derived cultures, ADH6-positive cells were absent or relatively weak, and where staining was detectable, it was predominantly associated with the mesodermal cellular component rather than an organized neuronal phenotype. Thus, the ADH6 pattern was consistent with incomplete progression of the ATN-associated transition in the patient cultures. These findings support the utility of ADH6 as a candidate metabolic marker for monitoring the ATN process, while not establishing a direct causal role for ADH6 in neuronal differentiation (Salehi et al., 2016; Sharma et al., 2022a).

SERCA2 showed a broader expression pattern across both neuronal and mesodermal components, indicating preservation of calcium-handling-associated cellular characteristics during lineage remodelling. A spatial difference was nevertheless evident between the two PITTRep microenvironments. In the coverslip-associated regions, SERCA2 expression was observed across the earlier differentiating cellular population, whereas under the hypoxia-associated well condition, SERCA2 expression was more predominently associated with the neuronal phenotype. The stronger neuronal association of SERCA2 under the well-associated condition occurred alongside increased neuronal representation, suggesting an association between SERCA2 expression and progression toward the neuronal phenotype within the PITTRep microenvironment (Britzolaki et al., 2018; Sun et al., 2022; Cornelio-Martínez and Lagunas-Rangel, 2026).

Quantitative assessment of ADH6 and SERCA2 fluorescence, including measurements within the corresponding ADH6–SERCA2 co-expressing regions, was also performed under coverslip and well-associated culture conditions (Supplementary Figure S6).

Collectively, the nM phenotype, together with the altered ADH6 distribution and the microenvironment-dependent SERCA2 pattern, demonstrates a distinct functional difference in ATN-associated remodelling in this GJB2-associated patient. Rather than interpreting these findings as evidence of a direct molecular mechanism, the results indicate that patient-derived PITTRep cultures can resolve differences in lineage progression and cellular phenotype that are not captured by the genetic diagnosis alone. This provides a functional genotype–phenotype framework for comparing the three GJB2 cases investigated in the present study.

Representative multispectral optoacoustic tomography (MSOT) maps of patient-, mother-, and father-derived PITTRep cultures are shown in the three columns. The rows depict deoxygenated haemoglobin (Hb), oxygenated haemoglobin ($HbO_2$), the combined Hb/$HbO_2$ distribution, total haemoglobin (HbT), and MSOT-derived mean oxygen saturation ($mSO_2$), respectively. Hb and $HbO_2$ maps demonstrate the spatial distribution of deoxygenated and oxygenated haemoglobin signals, while the combined Hb/$HbO_2$ maps illustrate their spatial relationship. HbT represents the combined haemoglobin signal derived from Hb and $HbO_2$, whereas $mSO_2$ represents the relative oxygen saturation estimated from $HbO_2$/HbT. Compared with the parental cultures, the patient-derived culture showed reduced and more spatially heterogeneous Hb and $HbO_2$ signals, a lower HbT-associated signal, and a distinct spatial distribution of $mSO_2$. These findings demonstrate differences in haemoglobin-associated signal distribution and

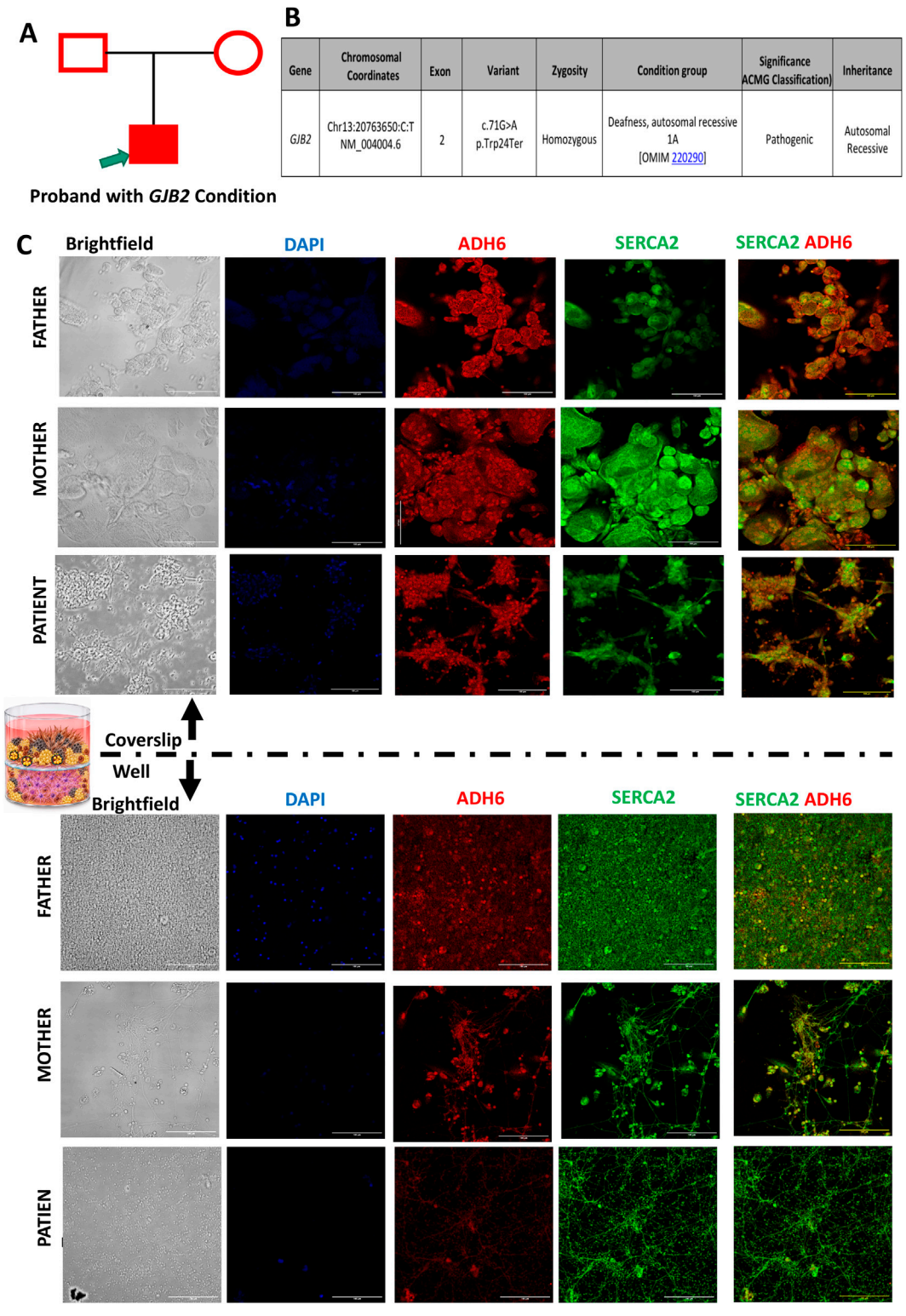


FIGURE 5
Patient-Specific disease Modeling Reveals Impaired Adipocyte-to-Neuronal Transdifferentiation in GJB2-Associated Congenital Sensorineural Hearing Loss **(A)** Family pedigree demonstrating autosomal recessive inheritance of congenital severe sensorineural hearing loss (SNHL) associated with a pathogenic GJB2 variant in the proband. **(B)** Whole-exome sequencing identified a homozygous pathogenic GJB2 variant [c.71G>A; p. Trp24Ter] associated with autosomal recessive deafness type 1A. **(C)** Immunofluorescence-based functional characterization of patient-derived PITTRep cultures in coverslip-associated normoxic microenvironment and standard well conditions (hypoxic) using ADH6, SERCA2, and DAPI. Parental controls demonstrated organized neuronal-network formation and efficient adipocyte-to-neuronal transdifferentiation (ATN), whereas patient-derived cultures exhibited disrupted neuronal architecture, reduced hypoxia-associated neurogenic remodelling, and altered metabolic-neurodevelopmental signaling. Composite images demonstrate reduced neuronal integration and defective lineage-associated organization within the patient-derived system compared with parental controls.

oxygenation patterns between the patient-derived and parental PITTRep cultures. MSOT-Based Assessment of Neurovascular Coupling in GJB2-Associated PITTRep Cultures.

## Case study V: MSOT-based assessment of neurovascular coupling in GJB2-associated PITTRep cultures

As a complementary functional assessment of the patient-specific PITTRep phenotype, we examined haemoglobin-associated signal distribution and oxygenation-related patterns in GJB2-associated cultures using multispectral optoacoustic tomography (MSOT). MSOT is a label-free imaging modality that uses pulsed optical excitation and ultrasound detection to visualize endogenous optical absorbers, including oxygenated haemoglobin (HbO2_22) and deoxygenated haemoglobin (Hb). Spectral unmixing enables estimation of Hb, HbO2_22, total haemoglobin (HbT = Hb + HbO2), and MSOT-derived oxygen saturation (mSO2 = HbO2/HbT) (Karlas et al., 2021a; 2021b; Regensburger et al., 2024).

The rationale for this analysis derives from the central role of connexin-based gap junctions in intercellular communication and the observation that endothelial connexin coupling can govern the propagation, speed, and spatial extent of neurally evoked vasodilation *in vivo* (Krolak et al., 2025). However, this evidence concerns endothelial Cx37/Cx40 in mouse brain vasculature and is used here only as general biological context; it does not establish a direct role of GJB2/Cx26 in the haemoglobin-related patterns observed in PITTRep cultures.

MSOT provides label-free visualization of endogenous haemoglobin signals and enables assessment of deoxygenated haemoglobin (Hb), oxygenated haemoglobin ($HbO_2$), total haemoglobin (HbT), and MSOT-derived oxygen saturation ($mSO_2$). In the present study, these parameters were compared between the patient-derived culture and biologically related parental control cultures to assess differences in vascular representation and oxygenation-associated patterns (Karlas et al., 2021b; Regensburger et al., 2024).

The patient-derived culture demonstrated markedly reduced Hb and $HbO_2$ signals compared with the parental cultures, together with a substantially reduced HbT-associated signal and altered $mSO_2$ distribution (Figure 6). Importantly, the spatial relationship between oxygenated and deoxygenated haemoglobin signals appeared substantially less organized in the patient-derived culture than in the parental controls. The comparatively limited and spatially heterogeneous haemoglobin distribution suggested reduced coordination between the neurovascular components of the patient-derived tissue-like culture.

When considered alongside the predominantly nM cellular phenotype and reduced neuronal representation observed by immunofluorescence, the MSOT findings provide a complementary patient-specific functional phenotype. In the present exploratory comparison, the patient-derived culture showed reduced Hb and HbO222 signals relative to parental cultures, lower HbT-associated signal, and spatially altered mSO222 distribution (Figure 6). The spatial relationship between HbO222 and Hb signals also appeared less organised in the patient-derived culture. These findings indicate a difference in haemoglobin-associated signal distribution and oxygenation-related patterning in the GJB2-associated PITTRep culture.

These observations should be regarded as preliminary evidence of an altered neurovascular/haemodynamic phenotype relevant to neurovascular coupling, rather than direct proof of impaired neurovascular coupling. Larger studies incorporating quantitative region-of-interest analysis, biological replicates, endothelial-marker validation, and dynamic measurements that link neuronal activity with haemodynamic responses will be required to establish reproducibility, cellular identity, and mechanism.

Importantly, these MSOT observations should be considered preliminary functional evidence rather than definitive proof of impaired neurovascular coupling. The present analysis was designed to explore whether a patient-specific neurovascular phenotype could be detected in the PITTRep system, and further studies incorporating larger numbers of GJB2-associated cultures and quantitative measures of vascular and neuronal coupling will be required to establish the reproducibility and biological significance of this finding. Nevertheless, the observed difference provides an additional functional layer linking the patient's GJB2 genotype with altered cellular and neurovascular phenotypes in the patient-derived model.

## Case study VI: Intrafamilial functional characterisation of progressive GJB2-associated hearing loss

To further examine the relationship between the GJB2 genotype, clinical phenotype, and patient-derived functional phenotype, four affected individuals from the same family carrying the heterozygous c.551G>A; p. Arg184Gln (R184Q) variant were evaluated using the PITTRep platform (Figures 7, 8). All individuals exhibited a progressive moderate to severe hearing-loss phenotype, providing an opportunity to examine patient-derived cellular characteristics within a shared genetic and familial background (Su et al., 2010).

In contrast to the congenital profound hearing-loss phenotype associated with the truncating GJB2 variant described in the preceding case, these individuals demonstrated a progressive auditory phenotype associated with the R184Q missense variant. The PITTRep cultures provided an additional functional layer for examining whether differences in lineage-associated remodelling could be detected alongside the clinical phenotype.

Based on the lineage nomenclature established in the earlier GJB2 case, both patient-derived cultures demonstrated a predominantly nM phenotype, indicating major mesodermal representation with relatively limited neuronal differentiation. This pattern was evident in comparison with healthy parental cultures, which showed greater neuronal-associated organization and more prominent remodelling under the stress-responsive well condition. The nM phenotype therefore suggests that the patient-derived cells retained substantial mesodermal characteristics but showed limited progression toward the neuronal state required for efficient ATN.

ADH6 provided an additional readout of this transition. As observed in the previous GJB2 case, ADH6-associated staining was considered in the context of the intermediate stage of adipocyte-to-neuronal transdifferentiation. Reduced or heterogeneous ADH6-associated staining in the patient-derived cultures was consistent with altered progression through this intermediate

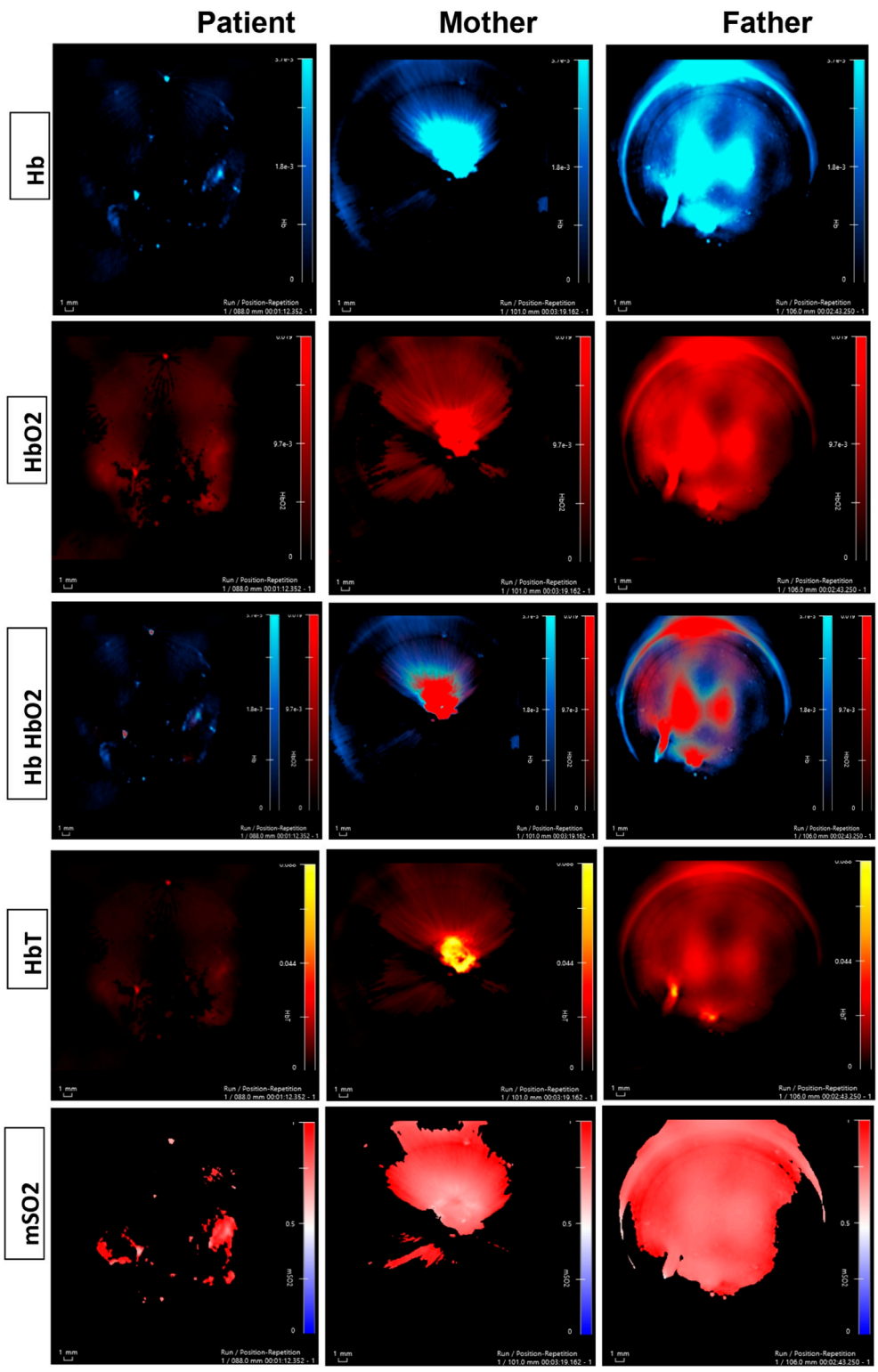


FIGURE 6
MSOT analysis of neurovascular and oxygenation patterns in GJB2-associated PITTRep cultures.

metabolic/retinoid-associated stage, rather than simply representing a generalised absence of cellular differentiation. This is relevant to the proposed ATN model because retinoid metabolism provides a potential metabolic component of lineage remodelling, and ADH6-associated expression may decrease as cells progress toward a more mature neuronal phenotype.

In contrast, SERCA2-associated expression remained detectable in the patient-derived cultures under both microenvironmental

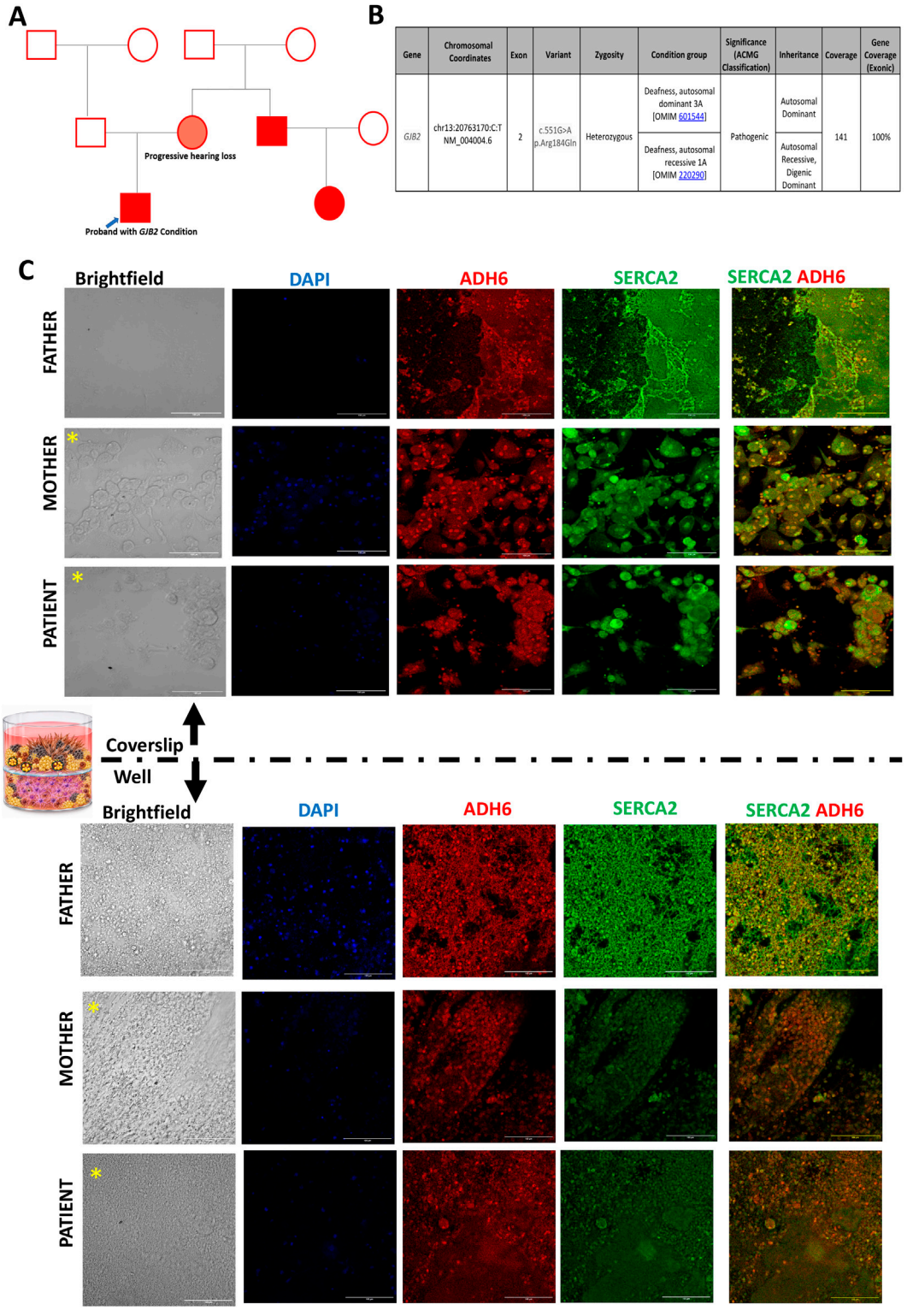


| Gene | Chromosomal Coordinates | Exon | Variant | Zygosity | Condition group | Significance (ACMG Classification) | Inheritance | Coverage | Gene Coverage (Exonic) |
|---|---|---|---|---|---|---|---|---|---|
| *GJB2* | chr13:20763170:C:T NM_004004.6 | 2 | c.551G>A p.Arg184Gln | Heterozygous | Deafness, autosomal dominant 3A [OMIM 601544] | Pathogenic | Autosomal Dominant | 141 | 100% |
| | | | | | Deafness, autosomal recessive 1A [OMIM 220290] | | Autosomal Recessive, Digenic Dominant | | |

FIGURE 7
Family-Specific Disease Modelling of Progressive moderate GJB2-Associated Sensorineural Hearing Loss Reveals Impaired Neurogenic Remodelling **(A)** Pedigree demonstrating familial occurrence of progressive moderate hearing loss. The proband and his mother exhibited the affected phenotype with variable clinical expressivity, with the mother showing a moderate degree of hearing impairment, while the proband demonstrated progressive moderate-to-severe hearing loss. **(B)** Whole-exome sequencing identified a heterozygous pathogenic GJB2 variant, c.551G>A; p. Arg184Gln (R184Q), located in exon 2 of GJB2. The variant has been reported in association with autosomal dominant nonsyndromic hearing loss 3A (DFNA3A). **(C)** Immunofluorescence characterisation of PITTRep-derived cultures from the father, mother, and patient with coverslip and well-associated microenvironmental conditions using ADH6, SERCA2, and DAPI. Compared with the father as a control, the patient's and his mother's blood-derived cultures demonstrated reduced neuronal-associated organisation and a predominantly nM phenotype, characterised by major mesodermal

*(Continued)*

FIGURE 7 (Continued)
representation with relatively limited neuronal differentiation. ADH6-associated staining was reduced and heterogeneous in the patient culture, while SERCA2-associated expression remained detectable across the cellular populations. The altered lineage-associated pattern was more evident under the well-associated stress-responsive condition, where the father, as a healthy control, showed greater structural organization and neuronal remodelling. Yellow asterisks indicate affected individuals with progressive hearing loss.

conditions. The persistence of SERCA2 staining suggests that cellular machinery was retained despite the altered lineage phenotype. However, its spatial distribution differed from that observed in the parental controls, particularly in relation to the neuronal-associated structures. Thus, the findings suggest that altered cellular organization may accompany, rather than completely prevent, the lineage transition.

Quantitative assessment of ADH6 and SERCA2 fluorescence, including measurements within the corresponding ADH6–SERCA2 co-expressing regions, was also performed under coverslip and well-associated culture conditions for both cases (Supplementary Figures S7 and S8).

The difference between the coverslip and well-associated conditions was also informative. The well microenvironment provides a more stress-responsive setting in which neuronal remodelling is more evident in control cultures. In the patient and her father's blood-derived cultures, however, this environmental stimulus did not result in a comparable increase in neuronal organization. Instead, the cultures retained the nM phenotype, suggesting a reduced capacity for stress-associated progression toward neuronal differentiation.

Nevertheless, the concordance of progressive moderate hearing loss with an nM PITTRep phenotype and altered ADH6/SERCA2-associated patterns provides an additional genotype–phenotype–functional layer. Together with the preceding truncating GJB2 case, these observations suggest that different clinical presentations of GJB2-associated hearing loss may be accompanied by distinct degrees of disruption in patient-specific neurogenic plasticity and ATN-associated remodelling.

## Case study VII: FGF3-associated congenital hearing loss reveals impaired FGF signalling and neurogenic plasticity

The final case involved a 1-year-old male with bilateral congenital severe-to-profound sensorineural hearing loss (SNHL) and profound absence of auditory responsiveness since infancy. Clinical evaluation revealed developmental delay and craniofacial dysmorphism, including triangular facies, together with radiological evidence of severe congenital inner-ear malformation consistent with Michel's aplasia. Auditory brainstem response (ABR) testing demonstrated complete absence of reproducible auditory waveforms, with no detectable response to electrical stimulation, indicating profound impairment of the auditory pathway (not shown). Given the severe structural and functional involvement of the peripheral auditory system, auditory brainstem implantation (ABI) was performed to provide auditory stimulation beyond the malformed/non-functional peripheral auditory pathway. The combination of congenital severe-to-profound hearing loss, inner-ear developmental abnormality, developmental delay, and craniofacial features showed substantial clinical concordance with the reported spectrum of FGF3-associated developmental auditory disorders, in which severe congenital deafness may occur with inner-ear malformations and associated craniofacial abnormalities (Singh et al., 2014; Urness et al., 2018; Al Yassin et al., 2019).

Whole-exome sequencing identified a homozygous FGF3 c.534C>G; p. Phe178Leu variant, which was classified as a VUS in the genomic analysis (Figure 9). Although the molecular classification did not independently establish pathogenicity, the finding was considered relevant in view of the patient's highly concordant clinical phenotype. The same variant has previously been reported in association with FGF3-related labyrinthine aplasia, microtia and microdontia (LAMM) syndrome, and studies have demonstrated that FGF3 is essential for otic placode and inner-ear development (Singh et al., 2014; Urness et al., 2018).

This case therefore provided an opportunity to investigate whether the clinical phenotype associated with the FGF3 variant was accompanied by a measurable functional alteration in patient-derived cells. Patient blood-derived PITTRep cultures were evaluated under coverslip-associated and well-associated microenvironments to examine neurogenic remodelling and FGF-associated signalling. Unlike conventional genomic analysis, this approach allowed assessment of the cellular consequences associated with the patient's genotype in an autologous system.

Immunofluorescence analysis demonstrated altered FGF2 and phosphorylated FGFR2 (pFGFR2) expression in the patient-derived cultures compared with parental controls. FGF3 is a ligand within the FGF signalling pathway and can signal through FGFR2, particularly FGFR2b, during developmental processes including otic placode and inner-ear formation. Thus, pFGFR2 was examined as a downstream indicator of receptor-associated FGF signalling rather than as a direct measure of FGF3 itself. The altered FGF2/pFGFR2 pattern observed in the patient culture therefore suggests disturbance of FGF-associated signalling activity (Sharma et al., 2022b; Arora et al., 2025) (Figure 9).

This molecular alteration was accompanied by marked differences in cellular organization. Parental cultures demonstrated more organized tissue architecture and greater neuronal-like structural development, whereas the patient-derived cultures showed reduced organization and impaired progression toward neuronal-like states. Within the PITTRep framework, this was interpreted in the context of adipocyte-to-neuronal transdifferentiation (ATN), which represents the neurogenic plasticity being investigated across the patient cohort.

The findings are biologically relevant because FGF signalling has established roles in developmental patterning, cellular differentiation, proliferation, migration and survival. In particular, FGF3-dependent signalling is critical during early otic development, and disruption of this pathway can result in profound abnormalities of inner-ear formation. Therefore, the altered FGF2/pFGFR2

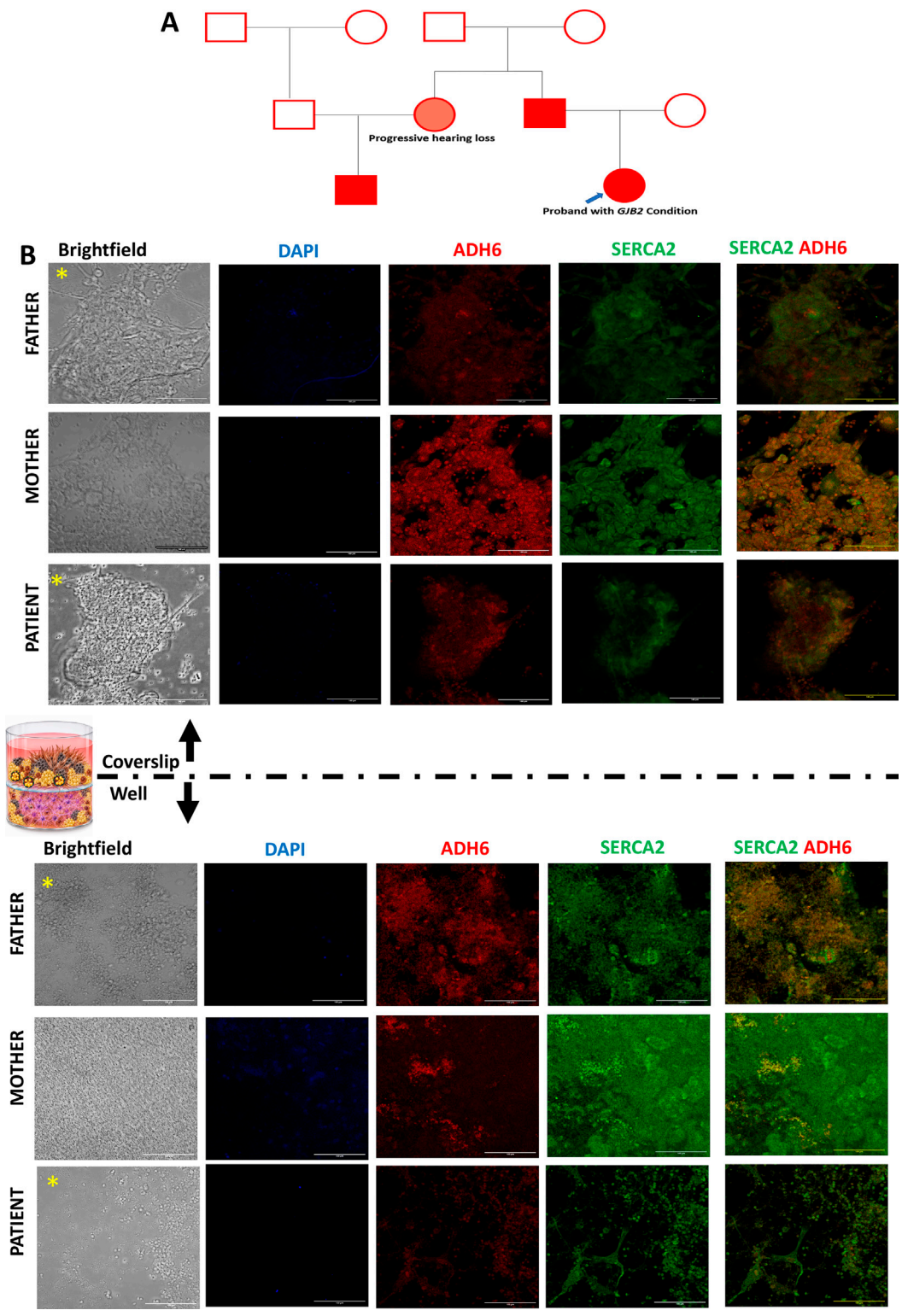


FIGURE 8
Patient-Specific Functional Characterization of Progressive GJB2-Associated Hearing Loss in the Same Family **(A)** Pedigree demonstrating familial occurrence of progressive moderate-to-severe hearing loss, with both the father and daughter affected. The clinical phenotypes demonstrate variable expressivity within the family, with progressive hearing impairment observed in both affected individuals. The affected proband was selected for patient-derived PITTRep analysis. **(B)** Immunofluorescence characterisation of PITTRep-derived cultures from the affected father, mother, and affected patient in coverslip and well-associated conditions using ADH6, SERCA2, and DAPI. The father's and patient-derived cultures demonstrated a predominantly nM phenotype, with greater mesodermal representation and reduced neuronal-associated organization compared with parental controls. ADH6 expression was comparatively reduced and heterogeneous, consistent with limited progression through the adipocyte-to-neuronal transdifferentiation pathway, whereas SERCA2-associated expression remained evident in both microenvironmental conditions. The findings provide a patient-specific cellular correlate of altered neurogenic remodelling in this affected member of the family. Yellow asterisks indicate affected individuals with progressive hearing loss.

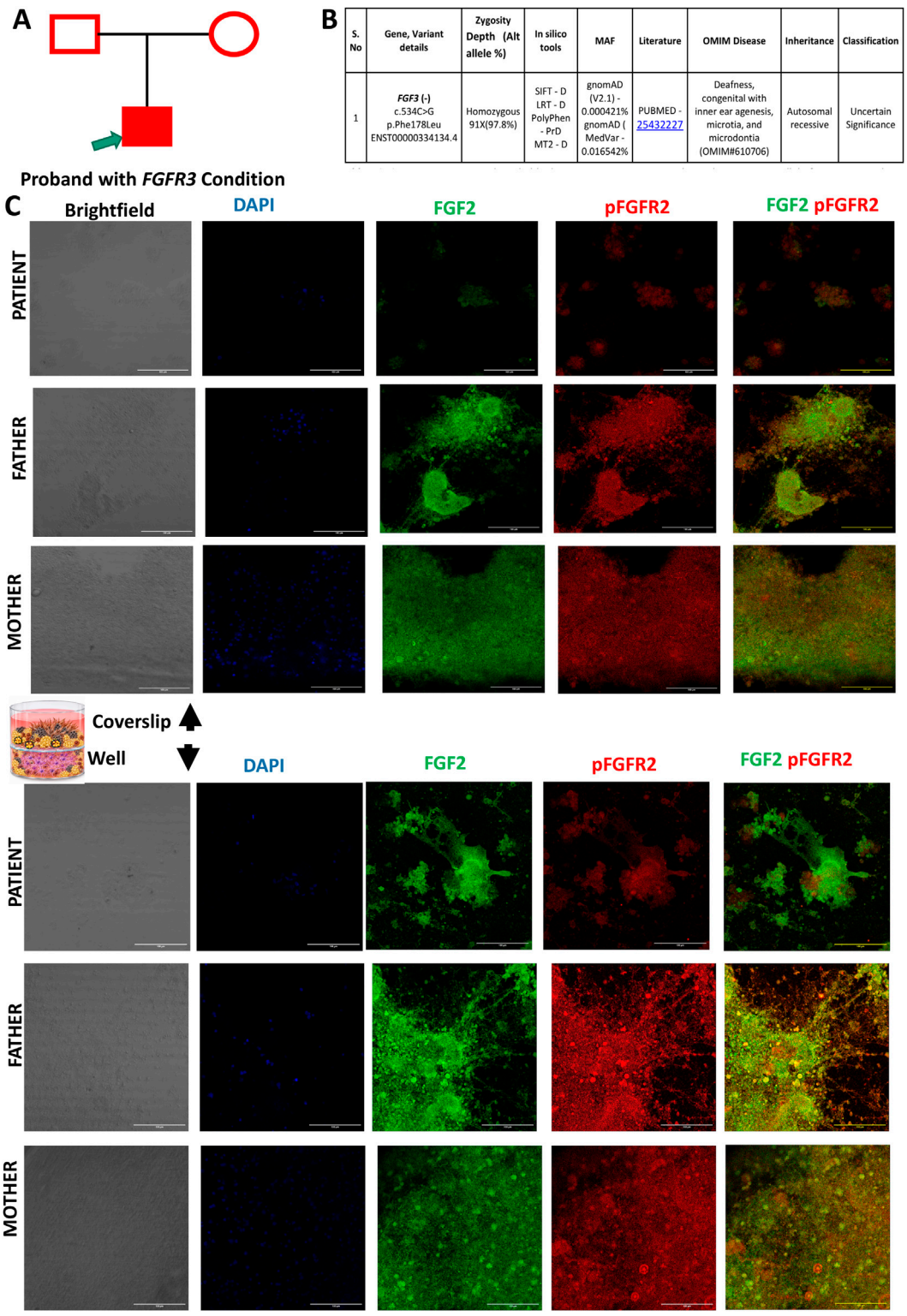


| S. No | Gene, Variant details | Zygosity Depth (Alt allele %) | In silico tools | MAF | Literature | OMIM Disease | Inheritance | Classification |
|---|---|---|---|---|---|---|---|---|
| 1 | *FGF3* (-) c.534C>G p.Phe178Leu ENST00000334134.4 | Homozygous 91X(97.8%) | SIFT - D LRT - D PolyPhen - PrD MT2 - D | gnomAD (V2.1) - 0.000421% gnomAD ( MedVar - 0.016542% | PUBMED - 25432227 | Deafness, congenital with inner ear agenesis, microtia, and microdontia (OMIM#610706) | Autosomal recessive | Uncertain Significance |

FIGURE 9
FGF3-Associated Congenital Sensorineural Hearing Loss with Impaired FGF Signalling and Neurogenic Plasticity **(A)**Pedigree demonstrating autosomal recessive inheritance, with the affected proband born to unaffected parents. **(B)**Whole-exome sequencing identified a homozygous FGF3 variant [c.534C>G; p. Phe178Leu], classified as a variant of uncertain significance (VUS). The variant was evaluated in the context of the patient's clinical phenotype and molecular findings. **(C)**Immunofluorescence-based characterization of patient-derived PITTRep cultures under coverslip-associated and well-associated microenvironments using FGF2, phosphorylated FGFR2 (pFGFR2), and DAPI. Compared with parental controls, the patient-derived cultures demonstrated altered FGF2 and pFGFR2 expression, reduced organization of neuronal-like structures, and impaired adipocyte-to-neuronal transdifferentiation (ATN). The findings indicate altered FGF-associated signalling and neurodevelopmental plasticity in the patient-derived system.

phenotype observed in the patient's PITTRep culture provides functional evidence consistent with altered FGF-associated signalling, although it should not by itself be interpreted as definitive proof that the FGF3 variant is pathogenic (Figure 9).

Quantitative assessment of FGF2 and phospho-FGFR2 fluorescence, including measurements within the corresponding FGF2–phospho-FGFR2 co-expressing regions, was also performed under coverslip and well-associated culture conditions (Supplementary Figure S9).

Importantly, the clinical-genetic-functional concordance in this case is notable. The patient exhibited a severe congenital auditory phenotype with structural inner-ear abnormalities; the FGF3 variant was identified in the homozygous state; and the patient-derived culture demonstrated altered FGF-associated signalling together with impaired neurogenic remodelling. Previous reports have also demonstrated that biallelic FGF3 variants can cause severe congenital deafness associated with inner-ear agenesis, supporting the biological plausibility of the observed phenotype.

### Limitations

This study has several limitations. First, the biological sample size was limited, as each case was represented by individual patient- and available parental/familial samples, with no independent biological or technical replicate cultures. Additional sample collection was also limited by the young age of the participants and the clinical feasibility of obtaining excess blood samples. Therefore, the immunofluorescence findings, particularly the quantitative comparisons, should be interpreted as exploratory and require validation in larger cohorts with independent biological replicates. Second, while quantitative immunofluorescence and MSOT-based assessments provided complementary cellular and functional observations, these findings remain preliminary and require validation through larger-scale studies incorporating additional quantitative molecular and functional assays. Overall, the present study should be considered a proof-of-concept demonstration of the potential of PITTRep cultures for patient-specific functional characterization and genotype–phenotype assessment, rather than definitive evidence of disease mechanisms.

## Conclusion

The present study demonstrates the utility of the Plasma-Induced Transcriptomic and Epitranscriptomic Reprogramming (PITTRep) platform for patient-specific functional modelling across seven clinically and genetically diverse cases of sensorineural hearing loss, encompassing POU3F4-, MYO7A-, and GJB2-associated hereditary hearing loss, FGF3-associated developmental hearing loss, and acquired ototoxic hearing loss without an identified disease-associated variant. Across these distinct clinical contexts, patient-derived cultures exhibited reproducible alterations in cellular organization and progression along the adipocyte-to-neurogenic transdifferentiation (ATN) continuum, supporting ATN-associated remodeling as a measurable functional phenotype of auditory-neural dysfunction. These observations extend our previous demonstration that autologous plasma can induce reproducible neurogenic remodeling in human blood-derived cells (Sharma et al., 2022b; Arora et al., 2025).

Importantly, the individual cases demonstrated distinct functional signatures rather than a uniform molecular phenotype. The POU3F4-associated case showed altered neuronal and developmental markers with partial modulation following artificial endolymph supplementation, highlighting the influence of the extracellular ionic environment on the patient-derived cellular state. The MYO7A-associated case demonstrated extensive regulatory remodeling accompanied by impaired progression through the ATN-associated trajectory, providing functional information beyond the identified coding variant. In the acquired ototoxic case, the absence of a significant phenotype-associated variant was accompanied by altered neurotrophic, inflammatory, and cytoskeletal features together with impaired neurogenic remodeling, demonstrating that the PITTRep phenotype can also be captured in an acquired form of SNHL.

The three GJB2-associated cases further illustrated the value of phenotype-specific functional stratification. The truncating GJB2 variant, c.71G>A; p. Trp24Ter, associated with congenital severe-to-profound hearing loss, showed an nM phenotype, indicating predominant mesodermal representation with limited neuronal progression. In contrast, the GJB2 R184Q-associated familial cases showed progressive hearing loss and a corresponding nM cellular phenotype, together with altered ADH6 distribution and microenvironment-dependent SERCA2 expression. ADH6 provided a candidate readout of the intermediate metabolic/retinoid-associated stage of ATN, whereas SERCA2 provided an additional readout of calcium-handling-associated cellular organization. These findings support the use of such markers for phenotypic characterization of ATN progression, without implying that either marker is itself causative.

The MSOT analysis provided an additional functional dimension in the GJB2 model by demonstrating differences in haemoglobin-associated signals, total haemoglobin distribution, and oxygenation patterns between patient-derived and parental cultures. Because connexins participate in intercellular communication and neurovascular signalling, this observation provides preliminary evidence that altered GJB2-associated cellular phenotypes may be accompanied by differences in neurovascular organization and oxygenation-associated responses within the PITTRep system. Importantly, these MSOT findings should be considered preliminary functional observations requiring validation in larger cohorts and with direct measures of coupling.

The final FGF3-associated case further demonstrated how PITTRep can complement genomic findings in a clinically concordant but molecularly unresolved setting. The homozygous c.534C>G; p. Phe178Leu variant was classified as a VUS, while the patient presented with severe congenital hearing loss, developmental abnormalities, craniofacial features, and severe inner-ear malformation. Altered FGF2 and phosphorylated FGFR2 expression, together with impaired neurogenic organization, provided a patient-specific functional phenotype consistent with altered FGF-associated signalling, although these findings do not independently establish variant pathogenicity.

Taken together, these findings indicate that genomic diagnosis and functional cellular phenotyping provide complementary levels of information. Genomic analysis identifies the underlying

genetic context, whereas PITTRep enables examination of how that context is reflected in patient-derived cellular remodeling, lineage progression, signalling responses, and microenvironmental adaptation. This distinction is particularly relevant for VUSs, clinically variable hereditary disorders, and acquired hearing loss in which conventional sequencing may not fully account for the observed phenotype. Such integration is consistent with the broader framework of precision medicine, in which multi-dimensional molecular and functional information can complement static genomic data (Ashley, 2016; Mani et al., 2025; Wang et al., 2023).

The principal strength of the present study is therefore not the establishment of a single molecular mechanism for SNHL, but the demonstration that patient-derived PITTRep cultures can reproducibly reveal disease-associated differences in neurogenic plasticity across heterogeneous auditory disorders. At the same time, the study is a proof-of-concept based on a limited number of clinically selected cases. The observed associations between genotype, signalling markers, ATN progression, and clinical phenotype should therefore not be interpreted as definitive causal relationships. Larger cohorts, quantitative phenotyping, longitudinal clinical correlation, and targeted perturbation studies will be required to determine the specificity and predictive value of these functional signatures.

Overall, this work establishes PITTRep as a complementary patient-specific functional modelling approach for SNHL, capable of linking genomic findings and clinical phenotypes with measurable cellular behavior using minimally invasive peripheral blood. Rather than replacing genomic diagnosis, PITTRep provides an additional functional layer that can help characterize unresolved or variable phenotypes and generate experimentally testable disease-associated cellular signatures. The reproducibility of altered ATN-associated remodeling across hereditary and acquired cases provides a foundation for further development of PITTRep as a functional platform for disease modelling and precision-oriented investigation of auditory-neural disorders.

## Data availability statement

The raw sequencing data is available from the NCBI Sequence Read Archive (SRA) database under accession number PRJNA1501410.

## Ethics statement

The studies involving humans were approved by Institutional Ethics Intramural Committee of the Postgraduate Institute of Medical Education and Research, IEC no: IEC-INT/2024/PhD-1585. Postgraduate institute of medical education and research, (PGIMER), Chandigarh, India. The studies were conducted in accordance with the local legislation and institutional requirements. Written informed consent for participation in this study was provided by the participants' legal guardians/next of kin. Written informed consent was obtained from the individual(s), and minor(s)' legal guardian/next of kin, for the publication of any potentially identifiable images or data included in this article.

## Author contributions

RA: Conceptualization, Data curation, Formal Analysis, Investigation, Methodology, Software, Validation, Visualization, Writing – original draft, Writing – review and editing. NP: Data curation, Formal Analysis, Methodology, Project administration, Resources, Supervision, Validation, Writing – review and editing. RV: Data curation, Formal Analysis, Methodology, Project administration, Resources, Supervision, Validation, Writing – review and editing. JB: Data curation, Formal Analysis, Methodology, Project administration, Resources, Supervision, Validation, Writing – review and editing. MD: Validation, Writing – original draft, Writing – review and editing. SK: Investigation, Software, Writing – original draft, Writing – review and editing. MS: Conceptualization, Data curation, Formal Analysis, Funding acquisition, Investigation, Methodology, Project administration, Resources, Software, Supervision, Validation, Visualization, Writing – original draft, Writing – review and editing.

## Funding

The author(s) declared that financial support was received for this work and/or its publication. This research was supported by the Science and Engineering Research Board (SERB), Government of India, through the CRG/2022/004946. Additional financial support was provided through PGIMER Intramural Research Grants (No.37602).

## Acknowledgments

The authors sincerely thank the patient and the patient's family for their participation, cooperation, and willingness to contribute to this research. Written informed consent for participation in the study and publication of anonymised clinical information and associated data was obtained from the patient's parent/legal guardian before study enrolment. Every effort has been made to protect patient privacy and confidentiality, and no personally identifiable information is disclosed in this manuscript. The authors also acknowledge the support of the Department of Otolaryngology and Head & Neck Surgery, Postgraduate Institute of Medical Education and Research (PGIMER), Chandigarh, and all laboratory personnel who contributed to sample collection, processing, and technical assistance. The authors acknowledge the use of free illsutration tools like smart servier, paint 3D microsoft, powerpoint, for generating the well-and-coverslip illustration used in this study, which was adapted by the authors to represent the experimental culture configuration. The "Integrated Multi-Modal Framework" illustration in Figure 2A (Panel F) was created using BioRender under an Academic Publication License. And for the BioRender figure itself, retain the required license citation: Created in BioRender. Arora, R. (2025) https://BioRender.com/cig124y.

## Conflict of interest

The author(s) declared that this work was conducted in the absence of any commercial or financial relationships that could be construed as a potential conflict of interest.

## Generative AI statement

The author(s) declared that generative AI was used in the creation of this manuscript. Artificial intelligence (AI)-assisted tools were used solely to improve the clarity, grammar and language of the manuscript during preparation. All scientific interpretations, experimental design, data analysis, conclusions, figure preparation, and the final manuscript content were critically reviewed, verified, and approved by the authors. The authors accept full responsibility for the accuracy, originality, and integrity of the work.

Any alternative text (alt text) provided alongside figures in this article has been generated by Frontiers with the support of artificial intelligence and reasonable efforts have been made to ensure accuracy, including review by the authors wherever possible. If you identify any issues, please contact us.

## Publisher's note

All claims expressed in this article are solely those of the authors and do not necessarily represent those of their affiliated organizations, or those of the publisher, the editors and the reviewers. Any product that may be evaluated in this article, or claim that may be made by its manufacturer, is not guaranteed or endorsed by the publisher.

## Supplementary material

The Supplementary Material for this article can be found online at: https://www.frontiersin.org/articles/10.3389/fmolb.2026.1922984/full#supplementary-material

## References


Agrawal, A., Balcı, H., Hanspers, K., Coort, S. L., Martens, M., Slenter, D. N., et al. (2024). WikiPathways 2024: next generation pathway database. *Nucleic Acids Res.* 52, D679–D689. doi: 10.1093/nar/gkad960

Al Yassin, A., D'arco, F., Morín, M., Pagarkar, W., Harrop-Griffiths, K., Shaida, A., et al. (2019). Three new mutations and mild, asymmetrical phenotype in the highly distinctive LAMM syndrome: a report of eight further cases. *Genes (Basel)* 10. doi: 10.3390/genes10070529

Amberger, J., Bocchini, C. A., Scott, A. F., and Hamosh, A. (2009). McKusick's online Mendelian inheritance in man (OMIM®). *Nucleic Acids Res.* 37, D793–D796. doi: 10.1093/nar/gkn665

Andrews, S. (2010). *FastQC: A quality control tool for high throughput sequence data. Babraham Bioinformatics*. Cambridge, United Kingdom: Babraham Institute. Available online at: https://www.bioinformatics.babraham.ac.uk/projects/fastqc/.

Antonijevic, M., Dallemagne, P., and Rochais, C. (2024). Inducing neuronal regeneration and differentiation via the BDNF/ TrkB signaling pathway: a key target against neurodegenerative diseases? *Neural Regen. Res.* 19, 495–496. doi: 10.4103/1673-5374.380896

Arora, R., Bhardwaj, A., Panda, N. K., Das, R., Sinharay, S., Patkulkar, P., et al. (2025). *Pro-Neurogenic Potential of Blood Cells Cultured in Autologous Plasma*. doi: 10.1101/2025.03.19.643269

Ashley, E. A. (2016). Towards precision medicine. *Nat. Rev. Genet.* 17, 507–522. doi: 10.1038/nrg.2016.86

Auton, A., Abecasis, G. R., Altshuler, D. M., Durbin, R. M., Bentley, D. R., Chakravarti, A., et al. (2015). A global reference for human genetic variation. *Nature* 526, 68–74. doi: 10.1038/nature15393

Basch, M. L., Brown, R. M., Jen, H. I., and Groves, A. K. (2016a). Where hearing starts: the development of the mammalian cochleia. *J. Anat.* 228, 233–254. doi: 10.1111/joa.123124

Basch, M. L., Brown, R. M., Jen, H. I., and Groves, A. K. (2016b). Where hearing starts: the development of the mammalian cochlea. *J. Anat.* 228, 233–254. doi: 10.1111/joa.12314

Bellon, A., Wegener, A., Lescallette, A. R., Valente, M., Yang, S. K., Gardette, R., et al. (2018). Transdifferentiation of human circulating monocytes into neuronal-like cells in 20 days and without reprograming. *Front. Mol. Neurosci.* 11, 323. doi: 10.3389/fnmol.2018.00323

Betschart, R. O., Riccio, C., Aguilera-Garcia, D., Blankenberg, S., Guo, L., Moch, H., et al. (2024). Biostatistical aspects of whole genome sequencing studies: preprocessing and quality control. *Biometrical J.* 66, e202300278. doi: 10.1002/bimj.202300278

Bohlson, S. S., and Tenner, A. J. (2025). Complement in the brain: contributions to neuroprotection, neuronal plasticity, and neuroinflammation. *Annu. Rev. Immunol. Downloaded* doi: 10.1146/annurev-immunol-101921

Bolger, A. M., Lohse, M., and Usadel, B. (2014). Trimmomatic: a flexible trimmer for Illumina sequence data. *Bioinformatics* 30, 2114–2120. doi: 10.1093/bioinformatics/btu170

Bovee, S., Klump, G. M., Köppl, C., and Pyott, S. J. (2024). The Stria vascularis: renewed attention on a key player in age-related hearing loss. *Int. J. Mol. Sci.* 25, 5391. doi: 10.3390/ijms25105391

Braunstein, E. M., Crenshaw, E. B., Morrow, B. E., and Adams, J. C. (2008). Cooperative function of Tbx1 and Brn4 in the periotic mesenchyme is necessary for cochlea formation. *JARO - J. Assoc. Res. Otolaryngology* 9, 33–43. doi: 10.1007/s10162-008-0110-6

Brazelton, T. R., Rossi, F. M. V., Keshet, G. I., and Blau, H. M. (2000). From marrow to brain: expression of neuronal phenotypes in adult mice. *Science* 290, 1775–1779. doi: 10.1126/science.290.5497.1775

Britzolaki, A., Saurine, J., Flaherty, E., Thelen, C., and Pitychoutis, P. M. (2018). The SERCA2: a gatekeeper of neuronal calcium homeostasis in the brain. *Cell. Mol. Neurobiol.* 38, 981–994. doi: 10.1007/s10571-018-0583-8

Brown, T. L., and Macklin, W. B. (2020). The actin cytoskeleton in myelinating cells. *Neurochem. Res.* 45, 684–693. doi: 10.1007/s11064-019-02753-0

Busby, L. C., Patrick, J. R., Lyons, L. W., and Martik, M. L. (2025). *Ectomesenchymal Identity Emerges via Relief of Twist1 Transcript Destabilization*. doi: 10.1101/2025.09.02.673848

Chuang, J.-H., Yang, W.-C., Lin, Y., and Glutamatergic Neurons, Y. (2021). Molecular sciences glutamatergic neurons differentiated from embryonic stem cells: an investigation of differentiation and associated. *Diseases*. doi: 10.3390/ijms

Clarke, D. J. B., Jeon, M., Stein, D. J., Moiseyev, N., Kropiwnicki, E., Dai, C., et al. (2021). Appyters: turning Jupyter notebooks into data-driven web apps. *Patterns (N Y)* 2 (3), 100213. doi: 10.1016/j.patter.2021.100213

Cornelio-Martínez, S., and Lagunas-Rangel, F. A. (2026). Hypoxia inducible factor-1α-driven signaling networks regulating adult neurogenesis *via* Notch, Wnt, and MAPK pathways. *Mol. Biol. Rep.* 53, 815. doi: 10.1007/s11033-026-11966-w

Cruz-Granados, P., Das, S., Bagheri-Loftabad, K., and Lopez-Escamez, J. A. (2025). A systematic review on the role of the Stria Vascularis in Menière's disease pathogenesis. *JARO - J. Assoc. Res. Otolaryngology* 26, 491–513. doi: 10.1007/s10162-025-01006-y

Davies, A., Zoubeidi, A., Beltran, H., and Selth, L. A. (2023). The transcriptional and epigenetic landscape of cancer cell lineage plasticity. *Cancer Discov.* 13, 1771–1788. doi: 10.1158/2159-8290.CD-23-0225

De Kok, Y. J. M., Van Der Maarel, S. M., Bitner-Glindzicz, M., Huber, I., Monaco, A. P., Malcolm, S., et al. (1995). Association between X-linked mixed deafness and mutations in the POU domain gene POU3F4. *Science* 267, 685–688. doi: 10.1126/science.7839145

Du, P., and Wang, J. (2025). Editorial overview: 3Rs update: a new era in cellular identity and therapeutic plasticity. *Curr. Opin. Genet. Dev.* 94, 102386. doi: 10.1016/j.gde.2025.102386

Eshraghi, A. A., Polineni, S. P., Davies, C., Shahal, D., Mittal, J., Al-Zaghal, Z., et al. (2020). Genotype-Phenotype correlation for predicting cochlear implant outcome: current challenges and opportunities. *Front. Genet.* 11, 678. doi: 10.3389/fgene.2020.00678

Esposito, M., Amory, J. K., and Kang, Y. (2024). The pathogenic role of retinoid nuclear receptor signaling in cancer and metabolic syndromes. *J. Exp. Med.* 221, e20240519. doi: 10.1084/jem.20240519

Fan, X., Hou, K., Liu, G., Shi, R., Wang, W., and Liang, G. (2025). Strategies to overcome the limitations of current organoid technology - engineered organoids. *J. Tissue Eng.* 16, 20417314251319475. doi: 10.1177/20417314251319475

Fetoni, A. R., Zorzi, V., Paciello, F., Ziraldo, G., Peres, C., Raspa, M., et al. (2018). Cx26 partial loss causes accelerated presbycusis by redox imbalance and dysregulation of Nfr2 pathway. *Redox Biol.* 19, 301–317. doi: 10.1016/j.redox.2018.08.002

Firth, H. V., Richards, S. M., Bevan, A. P., Clayton, S., Corpas, M., Rajan, D., et al. (2009). DECIPHER: database of chromosomal imbalance and phenotype in humans using ensembl resources. *Am. J. Hum. Genet.* 84, 524–533. doi: 10.1016/j.ajhg.2009.03.010

Flegel, C., Manteniotis, S., Osthold, S., Hatt, H., and Gisselmann, G. (2013). Expression profile of ectopic olfactory receptors determined by deep sequencing. *PLoS One* 8, e55368. doi: 10.1371/journal.pone.0055368

Flitsch, L. J., Laupman, K. E., and Brüstle, O. (2020). Transcription factor-based fate specification and forward programming for neural regeneration. *Front. Cell. Neurosci.* 14, 121. doi: 10.3389/fncel.2020.00121

Fokkema, I. F. A. C., Taschner, P. E. M., Schaafsma, G. C. P., Celli, J., Laros, J. F. J., and den Dunnen, J. T. (2011). LOVD v.2.0: the next generation in gene variant databases. *Hum. Mutat.* 32, 557–563. doi: 10.1002/humu.21438

Ganesan, P., Schmiedge, J., Manchaiah, V., Swapna, S., Dhandayutham, S., and Kothandaraman, P. P. (2018). Ototoxicity: a challenge in diagnosis and treatment. *J. Audiol. Otol.* 22, 59–68. doi: 10.7874/jao.2017.00360

Gascón, S., Masserdotti, G., Russo, G. L., and Götz, M. (2017). Direct neuronal reprogramming: achievements, hurdles, and new roads to success. *Cell Stem Cell* 21, 18–34. doi: 10.1016/j.stem.2017.06.011

Gouveia, R. P., Barreto, C. A. V., Melo, R., Carvalho, A. L., and Moreira, I. S. (2024). Exploring the impact of the stargazin V143L mutation on the dynamics of the AMPA receptor: stargazin complex. *Front. Cell. Neurosci.* 18, 1505846. doi: 10.3389/fncel.2024.1505846

Grillet, N., Schwander, M., Hildebrand, M. S., Sczaniecka, A., Kolatkar, A., Velasco, J., et al. (2009). Mutations in LOXHD1, an evolutionarily conserved stereociliary protein, disrupt hair cell function in mice and cause progressive hearing loss in humans. *Am. J. Hum. Genet.* 85, 328–337. doi: 10.1016/j.ajhg.2009.07.017

Groves, A. K., and Fekete, D. M. (2012). Shaping sound in space: the regulation of inner ear patterning. *Development* 139, 826. doi: 10.1242/dev

Han, J. H., Bae, S. H., Joo, S. Y., Kim, J. A., Kim, S. J., Jang, S. H., et al. (2024). Characterization of vestibular phenotypes in patients with genetic hearing loss. *J. Clin. Med.* 13, 2001. doi: 10.3390/jcm13072001

Harrison, S. M., Biesecker, L. G., and Rehm, H. L. (2019). Overview of specifications to the ACMG/AMP Variant Interpretation Guidelines. *Curr. Protoc. Hum. Genet.* 103, e93. doi: 10.1002/cphg.93

Hegde, S., Hegde, R., Kulkarni, S. S., Das, K. K., Gai, P. B., and Bulagouda, R. S. (2022). Analysis of genetic variations in connexin 26 (GJB2) gene among nonsyndromic hearing impairment: familial Study. *Glob. Med. Genet.* 09, 152–158. doi: 10.1055/s-0042-1743257

Hibino, H., Nin, F., Tsuzuki, C., and Kurachi, Y. (2010). How is the highly positive endocochlear potential formed? The specific architecture of the stria vascularis and the roles of the ion-transport apparatus. *Pflugers Arch.* 459, 521–533. doi: 10.1007/s00424-009-0754-z

Hilton, B. J., Griffin, J. M., Fawcett, J. W., and Bradke, F. (2024). Neuronal maturation and axon regeneration: unfixing circuitry to enable repair. *Nat. Rev. Neurosci.* 25, 649–667. doi: 10.1038/s41583-024-00849-3

Hobert, O. (2021). Homeobox genes and the specification of neuronal identity. *Nat. Rev. Neurosci.* 22, 627–636. doi: 10.1038/s41583-021-00497-x

Horschitz, S., Meyer-Lindenberg, A., and Schloss, P. (2010). Generation of neuronal cells from human peripheral blood mononuclear cells. *Neuroreport* 21, 185–190. doi: 10.1097/WNR.0b013e328334be4e

Hu, L., Chen, W., Qian, A., and Li, Y. P. (2024). Wnt/β-catenin signaling components and mechanisms in bone formation, homeostasis, and disease. *Bone Res.* 12, 39. doi: 10.1038/s41413-024-00342-8

Jafari-Raddani, F., Davoodi-Moghaddam, Z., Yousefi, A. M., Ghaffari, S. H., and Bashash, D. (2022). An overview of long noncoding RNAs: biology, functions, therapeutics, analysis methods, and bioinformatics tools. *Cell biochem. Funct.* 40, 800–825. doi: 10.1002/cbf.3748

Jumabay, M., Abdmaulen, R., Urs, S., Heydarkhan-Hagvall, S., Chazenbalk, G. D., Jordan, M. C., et al. (2012). Endothelial differentiation in multipotent cells derived from mouse and human white mature adipocytes. *J. Mol. Cell. Cardiol.* 53, 790–800. doi: 10.1016/j.yjmcc.2012.09.005

Karlas, A., Masthoff, M., Kallmayer, M., Helfen, A., Bariotakis, M., Fasoula, N. A., et al. (2021a). Multispectral optoacoustic tomography of peripheral arterial disease based on muscle hemoglobin gradients—a pilot clinical studies. *Ann. Transl. Med.* 9, 36. doi: 10.21037/atm-20-33221

Karlas, A., Masthoff, M., Kallmayer, M., Helfen, A., Bariotakis, M., Fasoula, N. A., et al. (2021b). Multispectral optoacoustic tomography of peripheral arterial disease based on muscle hemoglobin gradients—a pilot clinical study. *Ann. Transl. Med.* 9, 36. 36–36. doi: 10.21037/atm-20-3321

Keuls, R. A., Oh, Y. S., Patel, I., and Parchem, R. J. (2023). Post-transcriptional regulation in cranial neural crest cells expands developmental potential. *Proc. Natl. Acad. Sci. U. S. A.* 120, e2212578120. doi: 10.1073/pnas.2212578120

Kim, Y., and Choi, B. Y. (2022). Precision medicine approach to cochlear implantation. *Clin. Exp. Otorhinolaryngol.* 15, 299–309. doi: 10.21053/ceo.2022.01382

Kitama, T., Nishiyama, T., Hosoya, M., Shimanuki, M. N., Ueno, M., You, F., et al. (2025). Noise-Induced hearing loss: overview and future prospects for research on oxidative stress. *Int. J. Mol. Sci.* 26, 4927. doi: 10.3390/ijms26104927

Krolak, T., Kaplan, L., Navas, K., Chen, L., Birmingham, A., Ryvkin, D., et al. (2025). Brain endothelial gap junction coupling enables rapid vasodilation propagation during neurovascular coupling. *Cell* 188, 5003–5019.e22. doi: 10.1016/j.cell.2025.06.030

Kuleshov, M. V., Jones, M. R., Rouillard, A. D., Fernandez, N. F., Duan, Q., Wang, Z., et al. (2016). Enrichr: a comprehensive gene set enrichment analysis web server 2016 update. *Nucleic Acids Res.* 44, W90–W97. doi: 10.1093/nar/gkw377

Kumar, S., Sandell, L. L., Trainor, P. A., Koentgen, F., and Duester, G. (2012). Alcohol and aldehyde dehydrogenases: Retinoid metabolic effects in mouse knockout models. *Biochim. Biophys. Acta Mol. Cell Biol. Lipids* 1821, 198–205. doi: 10.1016/j.bbalip.2011.04.004

Landrum, M. J., Lee, J. M., Benson, M., Brown, G., Chao, C., Chitipiralla, S., et al. (2016). ClinVar: public archive of interpretations of clinically relevant variants. *Nucleic Acids Res.* 44, D862–D868. doi: 10.1093/nar/gkv1222

Larsen, E., Litvak, L. M., Liberman, M. C., and Maison, S. F. (2025). Peripheral neural plasticity in cochlear implant users across the lifespan. *JAMA Otolaryngol. Head. Neck Surg.* 152, 126. doi: 10.1001/jamaoto.2025.4050

Lennartsson, J., and Rönnstrand, L. (2012). STEM CELL FACTOR RECEPTOR/c-KIT: FROM BASIC SCIENCE TO CLINICAL IMPLICATIONS. *Clin. Implic. Physiol. Rev.* 92, 1619–1649. doi: 10.1152/phys

Li, H., and Durbin, R. (2010). Fast and accurate long-read alignment with Burrows-Wheeler transform. *Bioinformatics* 26, 589–595. doi: 10.1093/bioinformatics/btp698

Li, X., Wu, Z., Zhou, Q., and Lin, S. (2026). Cochlear inflammatory microenvironment in age-related hearing loss: mechanisms and recent advances. *Clin. Interv. Aging* 21, 590182. doi: 10.2147/CIA.S590182

Liu, J., Xiao, Q., Xiao, J., Niu, C., Li, Y., Zhang, X., et al. (2022). Wnt/β-catenin signalling: function, biological mechanisms, and therapeutic opportunities. *Signal Transduct. Target. Ther.* 7, 3. doi: 10.1038/s41392-021-00762-6

Lou, Y., Liu, Y., Wu, M., Jia, G., Xia, M., and Li, W. (2025). Inner ear organoids: recent progress and potential applications. *Fundam. Res.* 5, 2926–2936. doi: 10.1016/j.fmre.2023.07.013

Mammano, F. (2019). Inner ear connexin channels: roles in development and maintenance of cochlear function. *Cold Spring Harb. Perspect. Med.* 9. doi: 10.1101/cshperspect.a033233

Mani, S., Lalani, S. R., and Pammi, M. (2025). Genomics and multiomics in the age of precision medicine. *Pediatr. Res.* 97, 1399–1410. doi: 10.1038/s41390-025-04021-0

Marino, G. B., Wojciechowicz, M. L., Clarke, D. J. B., Kuleshov, M. V., Xie, Z., Jeon, M., et al. (2023). lncHUB2: aggregated and inferred knowledge about human and mouse lncRNAs. *Database* 2023, 2023. doi: 10.1093/database/baad009

Maßberg, D., and Hatt, H. (2018). HUMAN OLFACTORY RECEPTORS: NOVEL CELLULAR FUNCTIONS OUTSIDE OF THE NOSE. *Physiol. Rev.* 98, 1739–1763. doi: 10.1152/physrev.00013.2017.-Olfactory

McCarron, E. P., Stepien, K. M., Summerfield, N., Sharma, R., Jovanovic, A., Gossan, N., et al. (2026). Natural history of hearing loss in adults with mucopolysaccharidoses across phenotype and genotype. *Mol. Genet. Metab.* 148, 110140. doi: 10.1016/j.ymgme.2026.110140

McLaren, W., Pritchard, B., Rios, D., Chen, Y., Flicek, P., and Cunningham, F. (2010). Deriving the consequences of genomic variants with the Ensembl API and SNP Effect Predictor. *Bioinformatics* 26, 2069–2070. doi: 10.1093/bioinformatics/btq330

Meka, D. P., Scharrenberg, R., Zhao, B., Kobler, O., König, T., Schaefer, I., et al. (2019). Radial somatic F-actin organization affects growth cone dynamics during early neuronal development. *EMBO Rep.* 20, e47743. doi: 10.15252/embr.201947743

Mezey, E., Chandross, K. J., Harta, G., Maki, R. A., and McKercher, S. R. (2000). Turning blood into brain: cells bearing neuronal antigens generated *in vivo* from bone marrow. *Sci. (1979)* 290, 1779–1782. doi: 10.1126/science.290.5497.1779

Morris, J. A., Gonzalez, T., Blanton, S. H., Angeli, S. I., and Liu, X. Z. (2026). GJB2-Related hearing loss: Genotype-Phenotype correlations, natural history, and emerging therapeutic strategies. *Int. J. Mol. Sci.* 27, 491. doi: 10.3390/ijms27010491

Mottaz, A., David, F. P. A., Veuthey, A. L., and Yip, Y. L. (2010). Easy retrieval of single amino-acid polymorphisms and phenotype information using SwissVar. *Bioinformatics* 26, 851–852. doi: 10.1093/bioinformatics/btq028

Nagasaki, M., Yasuda, J., Katsuoka, F., Nariai, N., Kojima, K., Kawai, Y., et al. (2015). Rare variant discovery by deep whole-genome sequencing of 1,070 Japanese individuals. *Nat. Commun.* 6, 8018. doi: 10.1038/ncomms9018

Nin, F., Yoshida, T., Sawamura, S., Ogata, G., Ota, T., Higuchi, T., et al. (2016). The unique electrical properties in an extracellular fluid of the mammalian cochlea; their functional roles, homeostatic processes, and pathological significance. *Pflugers Arch.* 468, 1637–1649. doi: 10.1007/s00424-016-1871-0

Nusse, R., and Clevers, H. (2017). Wnt/β-Catenin signaling, disease, and emerging therapeutic modalities. *Cell* 169, 985–999. doi: 10.1016/j.cell.2017.05.016

Oza, A. M., DiStefano, M. T., Hemphill, S. E., Cushman, B. J., Grant, A. R., Siegert, R. K., et al. (2018). Expert specification of the ACMG/AMP variant interpretation guidelines for genetic hearing loss. *Hum. Mutat.* 39, 1593–1613. doi: 10.1002/humu.23630

Park, H., and Poo, M. M. (2012). Neurotrophin regulation of neural circuit development and function. *Nat. Rev. Neurosci.* 14, 7–23. doi: 10.1038/nrn3379

Phippard, D., Lu, L., Lee, D., Saunders, J. C., Bryan, E., and Iii, C. (1999). *Targeted Mutagenesis of the POU-Domain Gene Brn4/Pou3f4 Causes Developmental Defects in the Inner Ear*.

Pianigiani, G., and Roccio, M. (2024). Inner ear organoids: strengths and limitations. *JARO - J. Assoc. Res. Otolaryngology* 25, 5–11. doi: 10.1007/s10162-024-00929-2

Poplin, R., Ruano-Rubio, V., DePristo, M. A., Fennell, T. J., Carneiro, M. O., Van der Auwera, G. A., et al. (2017). *Scaling Accurate Genetic Variant Discovery to Tens of Thousands of Samples*. doi: 10.1101/201178

Regensburger, A. P., Eckstein, M., Wetzl, M., Raming, R., Paulus, L. P., Buehler, A., et al. (2024). Multispectral optoacoustic tomography enables assessment of disease activity in paediatric inflammatory bowel disease. *Photoacoustics* 35, 100578. doi: 10.1016/j.pacs.2023.100578

Richards, S., Aziz, N., Bale, S., Bick, D., Das, S., Gastier-Foster, J., et al. (2015a). Standards and guidelines for the interpretation of sequence variants: a joint consensus recommendation of the American College of Medical Genetics and Genomics and the Association for Molecular Pathologiy. *Genet. Med.* 17, 405–424. doi: 10.1038/gim.2015.310

Richards, S., Aziz, N., Bale, S., Bick, D., Das, S., Gastier-Foster, J., et al. (2015b). Standards and guidelines for the interpretation of sequence variants: a joint consensus recommendation of the American College of Medical Genetics and Genomics and the Association for Molecular Pathology. *Genet. Med.* 17, 405–424. doi: 10.1038/gim.2015.30

Richardson, G. P., de Monvel, J. B., and Petit, C. (2011). How the genetics of deafness illuminates auditory physiology. *Annu. Rev. Physiol.* 73, 311–334. doi: 10.1146/annurev-physiol-012110-142228

Roccio, M., and Edge, A. S. B. (2019). "Inner ear organoids: new tools to understand neurosensory cell development, degeneration and regeneration,", 146. Cambridge. doi: 10.1242/dev.177188*Development*

Salehi, H., Amirpour, N., Niapour, A., and Razavi, S. (2016). An overview of neural differentiation potential of human Adipose derived stem cells. *Stem Cell Rev. Rep.* 12, 26–41. doi: 10.1007/s12015-015-9631-7

Satokata, I., Ma, L., Ohshima, H., Bei, M., Woo, I., Nishizawa, K., et al. (2000). Msx2 deficiency in mice causes pleiotropic defects in bone growth and ectodermal organ formation.

Segal, D., and Dostie, J. (2023). The talented LncRNAs: meshing into transcriptional regulatory networks in cancer. *Cancers (Basel)* 15, 3433. doi: 10.3390/cancers15133433

Sharma, M., Vanam, H. P., Panda, N. K., Patro, S. K., Arora, R., Bhadada, S. K., et al. (2022a). Deciphering the neurosensory olfactory pathway and associated neo-immunometabolic vulnerabilities implicated in COVID-Associated mucormycosis (CAM) and COVID-19 in a diabeteis Backdrop—A novel perspective. *Diabetology* 3, 193–235. doi: 10.3390/diabetology30100123

Sharma, M., Vanam, H. P., Panda, N. K., Patro, S. K., Arora, R., Bhadada, S. K., et al. (2022b). Deciphering the neurosensory olfactory pathway and associated neo-immunometabolic vulnerabilities implicated in COVID-Associated mucormycosis (CAM) and COVID-19 in a diabetes Backdrop—A novel perspective. *Diabetology* 3, 193–235. doi: 10.3390/diabetology3010013

Sherry, S. T., Ward, M.-H., Kholodov, M., Baker, J., Phan, L., Smigielski, E. M., et al. (2001). dbSNP: the NCBI database of genetic variation.

Singh, A., Tekin, M., Falcone, M., and Kapoor, S. (2014). Delayed presentation of rickets in a child with labyrinthine Aplasia, microtia and microdontia (LAMM) syndrome.

Statello, L., Guo, C. J., Chen, L. L., and Huarte, M. (2021a). Gene regulations by long non-coding RNAs and its biological functions. *Nat. Rev. Mol. Cell Biol.* 22, 96–118. doi: 10.1038/s41580-020-00315-19

Statello, L., Guo, C. J., Chen, L. L., and Huarte, M. (2021b). Gene regulation by long non-coding RNAs and its biological functions. *Nat. Rev. Mol. Cell Biol.* 22, 96–118. doi: 10.1038/s41580-020-00315-9

Stenson, P. D., Mort, M., Ball, E. V., Evans, K., Hayden, M., Heywood, S., et al. (2017). The Human Gene Mutation Database: towards a comprehensive repository of inherited mutation data for medical research, genetic diagnosis and next-generation sequencing studies. *Hum. Genet.* 136, 665–677. doi: 10.1007/s00439-017-1779-6

Su, C. C., Li, S. Y., Su, M. C., Chen, W. C., and Yang, J. J. (2010). Mutation R184Q of connexin 26 in hearing loss patients has a dominant-negative effect on connexin 26 and connexin 30. *Eur. J. Hum. Genet.* 18, 1061–1064. doi: 10.1038/ejhg.2010.50

Sun, L., Gao, D., Chen, J., Hou, S., Li, Y., Huang, Y., et al. (2022). Failure of hearing acquisition in mice with reduced expression of connexin 26 correlates with the abnormal phasing of apoptosis relative to autophagy and defective ATP-Dependent Ca2+ signaling in Kölliker's organ. *Front. Cell. Neurosci.* 16, 816079. doi: 10.3389/fncel.2022.816079

Taliun, D., Harris, D. N., Kessler, M. D., Carlson, J., Szpiech, Z. A., Torres, R., et al. (2021). Sequencing of 53,831 diverse genomes from the NHLBI TOPMed Program. *Nature* 590, 290–299. doi: 10.1038/s41586-021-03205-y

Thulasiram, M. R., Ogier, J. M., and Dabdoub, A. (2022). Hearing function, degeneration, and disease: spotlight on the Stria Vascularis. *Front. Cell Dev. Biol.* 10, 841708. doi: 10.3389/fcell.2022.841708

Urizar, E., McCarron, E. P., Gadepalli, C., Bentley, A., Woolfson, P., Lin, S., et al. (2025). Genetic insights and diagnostic challenges in highly attenuated lysosomal storage disorders. *Genes (Basel)* 16, 915. doi: 10.3390/genes16080915

Urness, L. D., Wang, X., Doan, H., Shumway, N., Noyes, C. A., Gutierrez-Magana, E., et al. (2018). "Spatial and temporal inhibition of FGFR2b ligands reveals continuous requirements and novel targets in mouse inner ear morphogenesis,", 145. Cambridge. doi: 10.1242/dev.170142*Development*

van der Valk, W. H., Steinhart, M. R., Zhang, J., and Koehler, K. R. (2021). Building inner ears: recent advances and future challenges for *in vitro* organoid systems. *Cell Death Differ.* 28, 24–34. doi: 10.1038/s41418-020-00678-8

Vandenberghe, W., Nicoll, R. A., and Bredt, D. S. (2005). Stargazin is an AMPA receptor auxiliary subunit AMPA (-amino-3-hydroxy-5-methyl-4-isoxazolepropionic acid) receptors mediate fast excitatory synaptic transmission in brain and underlie aspects of synaptic plasticity. *Numerous AMPA Receptor-Binding Proteins Have Been Implicated AMPA Receptor Traffick-Ing Anchoring*. doi: 10.1073/pnas.0408269102

Vasan, L., Park, E., David, L. A., Fleming, T., and Schuurmans, C. (2021). Direct neuronal reprogramming: bridging the gap between basic science and clinical application. *Front. Cell Dev. Biol.* 9, 681087. doi: 10.3389/fcell.2021.681087

Verhoeven, K., Van Laer, L., Kirschhofer, K., Legan
refsep P. K., Hughes
refsep D. C., Schatteman, I., et al. (1998). Mutations in the human a-tectorin gene cause autosomal dominant non-syndromic hearing impairment.

Waissbluth, S., and Daniel, S. J. (2013). Cisplatin-induced ototoxicity: transporters playing a role in cisplatin toxicity. *Hear. Res.* 299, 37–45. doi: 10.1016/j.heares.2013.02.002

Wang, B., and Du, M. (2024). Increasing adipocyte number and reducing adipocyte size: the role of retinoids in adipose tissue development and metabolism. *Crit. Rev. Food Sci. Nutr.* 64, 10608–10625. doi: 10.1080/10408398.2023.2227258

Wang, W., Zhang, L. S., Zinsmaier, A. K., Patterson, G., Leptich, E. J., Shoemaker, S. L., et al. (2019). Neuroinflammation mediates noise-induced synaptic imbalance and tinnitus in rodent models. *PLoS Biol.* 17, e3000307. doi: 10.1371/journal.pbio.3000307

Wang, R. S., Maron, B. A., and Loscalzo, J. (2023). Multiomics network medicine approaches to precision medicine and therapeutics in cardiovascular diseases. *Arterioscler. Thromb. Vasc. Biol.* 43, 493–503. doi: 10.1161/ATVBAHA.122.318731

Wangemann, P. (2006). Supporting sensory transduction: cochlear fluid homeostasis and the endocochlear potential. *J. Physiology* 576, 11–21. doi: 10.1113/jphysiol.2006.112888

Weil, D., Blanchard, S., Kaplan, J., Guilford, P., Gibson, F., Walsh, J., et al. (1995). Defective myosin VIIA gene responsible for Usher syndrome type 1B. *Nature* 374 (6517), 60–61. doi: 10.1038/374060a0

Yáñez-Mó, M., Siljander, P. R., Andreu, Z., Zavec, A. B., Borràs, F. E., Buzas, E. I., et al. (2015). Biological properties of extracellular vesicles and their physiological functions. *J. Extracell. Vesicles* 4, 27066. doi: 10.3402/jev.v4.27066

Zhao, S., Agafonov, O., Azab, A., Stokowy, T., and Hovig, E. (2020). Accuracy and efficiency of germline variant calling pipelines for human genome data. *Sci. Rep.* 10, 20222. doi: 10.1038/s41598-020-77218-4

Zhu, Y., Chen, J., Liang, C., Zong, L., Chen, J., Jones, R. O., et al. (2015). Connexin26 (GJB2) deficiency reduces active cochlear amplification leading to late-onset hearing loss. *Neuroscience* 284, 719–729. doi: 10.1016/j.neuroscience.2014.10.061

Zuk, P. A., Zhu, M., Ashjian, P., De Ugarte, D. A., Huang, J. I., Mizuno, H., et al. (2002). Human adipose tissue is a source of multipotent stem cells. *Mol. Biol. Cell* 13, 4279–4295. doi: 10.1091/mbc.E02-02-0105